

Green Williamson enhancement of the hydrophobic properties of cellulose fibers: thermodynamic study and application to elaborate rosemary essential oil (REO) biodegradable plastic cocervates

El-Hammi Hayat, El Barkany Soufian, Jabir Loubna, Azougagh Omar, Jilal Issam, Achalhi Nafea, Salhi Amine, El Idrissi Abderrahmane, El Ouardi Youssef, Abou-Salama Mohamed, Laatikainen Katri

This is a Author's accepted manuscript (AAM) version of a publication
published by Springer
in Cellulose

DOI: 10.1007/s10570-024-05759-2

Copyright of the original publication:

© Springer Nature

Please cite the publication as follows:

El-Hammi, H., El Barkany, S., Jabir, L. et al. (2024). Green Williamson enhancement of the hydrophobic properties of cellulose fibers: thermodynamic study and application to elaborate rosemary essential oil (REO) biodegradable plastic cocervates. *Cellulose*. DOI: 10.1007/s10570-024-05759-2

**This is a parallel published version of an original publication.
This version can differ from the original published article.**

1 **Green Williamson enhancement of the hydrophobic properties of cellulose fibers:**
2 **thermodynamic study and application to elaborate rosemary essential oil (REO)**
3 **biodegradable plastic coacervates**

4 Hayat El-Hammi^{a*}, Soufian El Barkany^{a*}, Loubna Jabir^a, Omar Azougagh^a, Issam Jilal^b, Nafea Achalhi^c,
5 Amine Salhi^d, Abderrahmane El Idrissi^c, Youssef El Ouardi^e, Mohamed Abou-Salama^a, Katri
6 Laatikainen^e

7 ^aLaboratory of Molecular Chemistry, Materials and Environment (LMCME), Department of Chemistry,
8 Multidisciplinary Faculty of Nador, Mohamed 1st University, P. B. 300, 62700 Nador, Morocco

9 ^bLIMOME Laboratory, Faculty of Sciences Dhar El Mehraz, Sidi Mohamed Ben Abdellah University, B.P. 1796,
10 30000 Atlas, Fes, Morocco

11 ^cLaboratory Applied Chemistry and Environmental (LCAE-URAC18), Faculty of Sciences of Oujda, Mohamed
12 1st University, 60000 Oujda, Morocco

13 ^dApplied Chemistry Unit, Sciences and Technologies Faculty, Abdelmalek Essaadi University, 32 003 Al
14 Hoceima, Morocco

15 ^eLaboratory of Separation Technology, Lappeenranta University of Technology, P.O. Box 20, 53851
16 Lappeenranta, Finland

17 *Corresponding authors. E-mail addresses: el.barkany011@gmail.com (Soufian El Barkany),
18 hayat.elhammi7@gmail.com (Hayat El-Hammi)

19 **Abstract:**

20 In this paper, the dispersion encapsulation was investigated as new process to elaborate the
21 principal active (PA) loaded biodegradable plastic coacervates, which designs a model of vector
22 system and drug delivery matrix. The Rosemary Essential Oil (REO) (~ 54%w) was wrapped,
23 as PA-model, in Benzyl cellulose acrylate (BCac, DSBnz ~ 1.4 and DSAcr ~ 0.4) coacervates
24 that elaborated in the dispersing aqueous phase as new cellulose derivative. The advantage of
25 this modification is to ensure the transition from hydrophilic to hydrophobic character of the
26 cellulosic shell during the encapsulation process, which leads to encapsulation in one step.
27 Indeed, during the reaction, the dispersive forces, generated by the grafting reaction, disturb the
28 hydrophilic character of the water-soluble cellulose acrylate (Cac0.4). Then, the hydrophobic
29 behavior, acquired by the grafted benzylic entities, increases the BCac-affinity to the organic
30 compounds (oily dispersed phase). Therefore, the migration of the resulting polymer chains to
31 the EO-rich (discontinuous) micellar dispersed phase, to form a biphasic micellar membrane,
32 is strongly suggested. Experimental investigations, such as the relationship between the degree
33 of substitution (DS) and the demixing behavior of the polymer solutions, are in good agreement
34 with the theoretical interpretations basing on the Flory–Huggins thermodynamic theory. The
35 results showed a high DS effect on the physicochemical properties, especially the molar Gibbs
36 free energy of mixing.

37 **Keywords:** Cellulose acrylate, Williamson, Encapsulation, Biodegradable plastic, Flory–Huggins,
38 Thermodynamics of polymers

39

40 **Introduction:**

41 As expected in our previous work (Chaouf et al. 2020), the low degree of substitution DS (~
42 0.4) of acrylation cellulose reaction (in urea-alkali-solution as a green solvent) showed drastic
43 changes in the surface charge and physicochemical properties of cellulose, especially the
44 negative charge density and the water solubility. The resulted water-soluble cellulose (Cac0.4),
45 as an ecofriendly and green polyelectrolyte, exhibited good flocculatrice properties to Cu(II) ions
46 and colloidal Fe(OH)₃ solutions. Recently, the low DS cellulose modification has been the
47 subject of many serious study areas as strategy for developing of new cellulosic mixed
48 derivatives-based materials. In this regard, the general philosophy is the disruption of polymeric
49 structural stability of cellulose, and therefore, acquiring a given solubility level in the usual
50 solvents (Miyamoto et al. 1985, 1995; Schnabelrauch et al. 1992; Clasen and Kulicke 2001;
51 Heinze and Koschella 2005; O'Brien et al. 2021; Molenveld and Slaghek 2022; Niederquell et
52 al. 2022; Shi et al. 2022). On the other side, the water solubility of cellulose derivatives
53 (resulting from the reduction of supramolecular H-bond interactions) will be the key-open to
54 wide research areas in front of cellulose chemistry and its applications. Hence, Cac0.4 can
55 constitute a broad industrial base with other famous cellulose derivatives such as hydroxyethyl
56 cellulose (HEC) and cellulose acetate (CA).

57 The “ecofriendly aspect” of cellulose and its derivatives constitute a major part of the modern
58 green wave industry, especially the pharmaceutical technology of drugs delivery systems
59 (DDS) (Damiri et al. 2022; Hosseini et al. 2022; Huo et al. 2022; Jain et al. 2022; Liu et al.
60 2022; Nabipour et al. 2022; Zuppolini et al. 2022). Indeed, spheroids and cellulose-based carrier
61 have shown excellent characteristics compared to other synthetic polymers, including ease of
62 administration (Barbu et al. 2021; Gupta et al. 2021; Kulkarni et al. 2022; Subramanian et al.
63 2022), nontoxicity (Popa et al. 2022; Zhang et al. 2022; Janmohammadi et al. 2023) and
64 biodegradability (Karimian et al. 2019; Wijaya et al. 2021). Thus, the tropism control of the
65 size and the supramolecular interactions, in cellulose-based carrier, allow the incorporation of
66 wide range of active ingredients, which can broaden several application fields to affect the
67 majority of industrial sectors (Karimian et al. 2019; Zoia et al. 2020; Weiss et al. 2021),
68 particularly the cosmetic (de Amorim et al. 2020; Mbituyimana et al. 2021; Amorim et al. 2022;
69 Nascimento et al. 2022), therapeutic (Kim et al. 2012; Wen and Oh 2015; Dai et al. 2019;
70 Kumari et al. 2021) and physiotherapy (Wang and Chen 2005; Mehta and MacGillivray 2022),
71 food (Nsor-Atindana et al. 2017; Amalraj et al. 2018; Liu et al. 2021; Razavi et al. 2022; Smaoui

72 et al. 2022), electronics and engineering industries (Adonijah Graham et al. 2020; de Amorim
73 et al. 2020; Hassabo et al. 2022), etc.

74 In pharmacology and medicine, cellulosic based delivery vectors and carriers (DVC) are
75 promising substitutes to the synthetic ones that are often expensive (Carvalho et al. 2019;
76 Sukumaran and Gopi 2021; Khalil et al. 2022). Recently, the literature has reported some
77 promising applications of cellulosebased DVC, mainly “the targeting” which is still achieved
78 with plastic polymers, noble metals or silicon nanoparticles or liposomes (Ivanova et al. 2018;
79 Klębowski et al. 2018; Castellanos et al. 2019; Rață et al. 2019; Zhang et al. 2019; Cadinoiu et
80 al. 2021; Gu et al. 2021; Lv et al. 2021; Fukuta and Kogure 2022; Raza et al. 2022). In addition,
81 recent studies have shown that cellulosic encapsulation can ensures and encompass the drug
82 vectorization requirements of therapeutic molecules, in particular the hydrophobic- hydrophilic
83 balance, which directly affects their solubility in the biological fluid and their membrane
84 diffusion (Kesharwani et al. 2022; Mohan et al. 2022; Qiao et al. 2022; Rezaei et al. 2022), the
85 increase in the accumulative distribution at the level of the target organ and the toxicity
86 reduction of healthy tissues (Cadinoiu et al. 2019; Ciolacu et al. 2020; Rata et al. 2021; Sheng
87 et al. 2021a, b; Chung et al. 2022; Karimian et al. 2022), the increase in the elimination time
88 (decrease in metabolism) (Bertsch et al. 2019; Su et al. 2019; Johnson et al. 2020) and the high
89 storage stability (Low et al. 2019; Raghav et al. 2021; Aw et al. 2022; Ho et al. 2022; Ma et al.
90 2022).

91 The antimicrobial, antioxidant and anticancer properties of Rosemary EO are mainly exploited
92 for various food industrial applications as preservative and spice or flavor ingredient (Saito et
93 al. 2004; Panda 2005; Ibarra et al. 2010), cosmetic and pharmaceutical products (Rodríguez-
94 Rojo et al. 2012) and medical applications as therapeutic agent and a potential complementary
95 agent in anticancer therapy (González-Vallinas et al. 2015; De Oliveira et al. 2019). It can also
96 be use as natural pesticides and insecticide (Feng et al. 2016), and to increase shelf life of food
97 products maintaining their quality during storage (El Fawal et al. 2019). However, to overcome
98 the limitations due to high volatility and sensitivity to environmental conditions during storage,
99 the encapsulation technique has got more accepted method to enhance its stability and release
100 rate control. Hence, to beat these limitations and to result a more effective REO coacervates,
101 the dispersion coacervation was investigated. The advantages of the present modification can
102 be summarized in the possibility of achieving the hydrophilic-hydrophobic transition of
103 cellulosic shells, as a new coacervation process, in one step. In comparison with other
104 encapsulation techniques which involve the different cellulosic derivatives CDs (simple and

105 mixed or mixed with other carbohydrates), the coacervation by dispersion, mentioned in this
106 article, consists of the modification of the starting HLB values of the polymer by the grafting
107 reaction. However, other CDs retain their HLBs, and encapsulation will only be carried out
108 according to density and invariable types of supramolecular interactions. (Sheng et al. 2021a,
109 b; Lukova et al. 2023).

110 In this paper, the green Williamson etherification reaction of cellulose was carried out
111 successfully in aqueous-alkaline medium (NaOH) without any catalyst. Then, the challenge of
112 avoiding the use of expensive and toxic solvation systems for the modification of cellulose has
113 been achieved, and this by the prior incorporation and at low DS (0.4) of the acrylate entities.
114 The synthesis of Benzylcellulose Acrylate (BCac0.4), as a new cellulose derivative, was
115 successfully carried out in aqueous medium, and the proposed structures were confirmed based
116 on the structural vibrational (FTIR-ATR) and magnetic nuclear (^1H NMR and ^{13}C NMR-APT)
117 analysis. In addition, the thermal stability and the morphology changes were studied according
118 to the thermogravimetric analysis (TGA-drTG) thermograms and Scanning Electron
119 Microscopy (SEM), respectively. The crystalline compartment and the surface elemental
120 profile deviations of samples were recorded and studied using the X-ray diffraction
121 diffractograms and energy dispersive X-ray (EDX) spectra, respectively. The contact angle was
122 investigated to prove the positive occurrence of aqueous Williamson hydrophobization reaction
123 of cellulose. The supramolecular modifications of the cellulosic chain, during the Williamson
124 reaction and during the formation of the cellulose mixed derivative, was investigated to the
125 preparation of the coated REO as biodegradable cellulose-based carriers and drug delivery
126 systems. In addition, the new process was investigated along the encapsulation of Rosemary
127 Essential Oil (REO), as a bioactive molecule model, in BCac0.4 carrier using “dispersive
128 coacervation” (D-Coac). The D-Coac process consists in stabilizing micellar emulsions by
129 grafting reactions, where the polymer to be modified (originally hydrophilic) is dissolved in the
130 dispersing phase (water), while the dispersed phase (micelle) is constituted by the organic phase
131 which assembles the active principle and the monomer to be grafted. During the reaction, the
132 grafting step affects drastically the physicochemical properties of the polymer (Cac0.4),
133 especially the hydrophilic character that disappears gradually increasing the DS value of the
134 hydrophobic grafting entities. The reaction mixture becomes cloudier indicating the
135 hydrophobic adsorption of BCac0.4 on the micellar walls, thus forming a sort of membrane
136 Pickering at the biphasic interfacial level. Then, the accumulation of BCac0.4 and the evolution
137 of the reaction progress favor the demixation and the coacervation, which break the dispersive

138 equilibrium forces and cause the precipitation of the white sandy powder (coacervates) with
139 plastic aspect, indicating that the encapsulation of REO in BCac0.4 has been successfully
140 carried out. The results were in good agreement with those predicted according to the Flory–
141 Huggins thermodynamic theory (developed in the section theory and application), which
142 investigated to predict the demixation behavior of the cellulosic polymer solution during the
143 grafting reaction (Abderahmane et al. 2011; Jilal et al. 2018a, b; Jilal et al. 2018a, b).

144 To the best of our knowledge, the dispersive coacervation as new coating process by micellar
145 interfacial modification of cellulose, and the synthesis of Benzyl cellulose acrylate or its
146 application were never discussed in the literature, where the novelty and significance of this
147 work.

148 **Materials and Methods**

149 *Materials*

150 Rosemary Essential Oil (REO) was extracted by hydrodistillation from fresh rosemary leaves
151 (*Rosmarinus officinalis L.*) from the eastern region of Morocco (Taourirt). Microcrystalline
152 Cellulose (MCC) powder was obtained from HIMEDIA Company, the MCC molecular weight
153 ($M_w \sim 35.5 \cdot 10^3$ Da) and degree of polymerization ($DP_w \sim 220$) were estimated in (6%NaOH,
154 4%Urea, 90%H₂O) solvent system using Mark-Houwink equation where the intrinsic viscosity
155 was evaluated by an *Ubbelohde*-viscometer. Acrylamide (C₃H₅NO), NaOH, Urea, Sodium
156 Dodecyl Sulfate (SDS) and Benzyl bromide were purchased from Sigma Aldrich. All chemicals
157 and solvents are of analytical grade and were used as received without any further purification.

158 *Methods*

159 *Instrumental analysis*

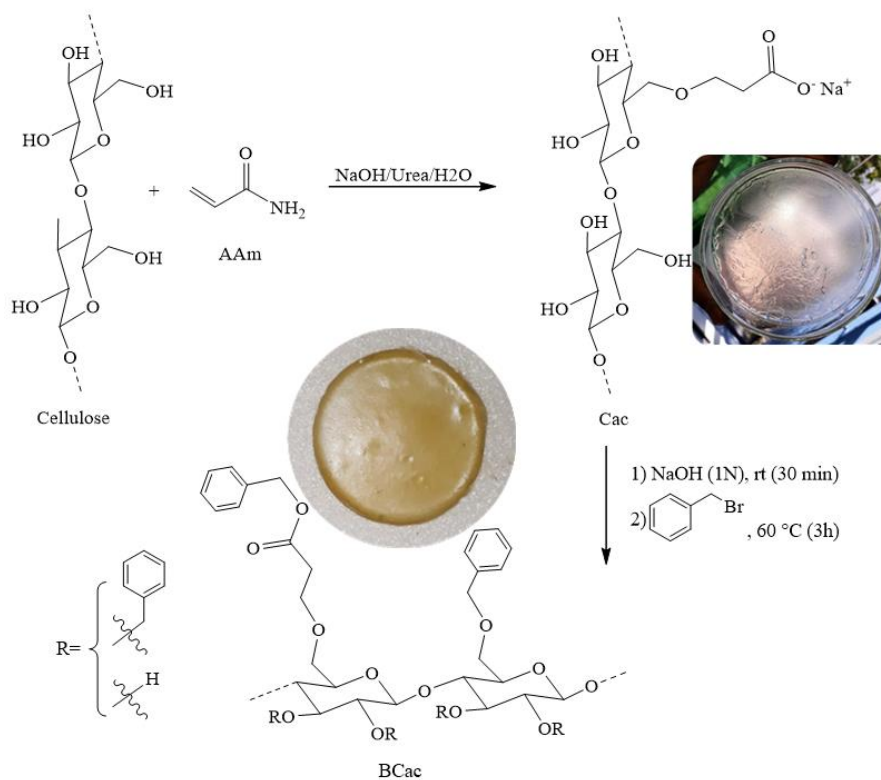
160 The vibrational (FTIR-ATR) spectra were recorded on *JASCOFT/IR-4700-ATR Spectrometer*,
161 and 40 scans were accumulated for each sample between 4000 and 400 cm⁻¹ to investigate the
162 proposed chemical structures. ¹H and ¹³C NMR-APT spectra were registered at 300 K on a
163 *BrukerAvance 400 MHz* spectrometer in DMSO-d₆ using TMS as an internal standard. The
164 crystalline profile changes were evaluated using X-ray diffraction technique and the patterns
165 were recorded on X-ray Diffractometer *EQUINOX 2000* using CuK α radiation ($\lambda = 1.5418 \text{ \AA}$),
166 at 40 kV and 30 mA as an accelerating voltage and an operating current, respectively. The
167 thermogravimetric analyses (TGA/DrTGA) were recorded to examine the thermal stability
168 behaviors of unmodified cellulose, its derivatives (water-soluble cellulose acrylate (Cac0.4) and
169 hydrophobic benzylated cellulose (BCac0.4)) and encapsulated matrix. The benzylated Cac

170 (BCac) and EOs loaded BCac (BCac-Oil) thermograms were registered on *Shimadzu DTG-60*
171 *simultaneous DTA-TG apparatus*, the scans were run from room temperature to 600 °C, at rate
172 of 10 °C/min under N₂ purge 50 ml. min⁻¹. The scanning electron microscopy (SEM) coupled
173 to the energy dispersive X-ray (EDX) were investigated to follow the effect of the chemical
174 modification on the surface morphologies, the microstructures and the superficial elemental
175 profile that summarized the different surface chemical elements. The SEM images and the EDX
176 spectra were obtained using *TESCAN VEGA 3 LM* microscope at accelerating voltage of 10 kV.
177 Contact angle values were measured using smartphone camera fixed to an optical device
178 developed in the laboratory. Briefly, a small drop of deionized water (0.5 to 3 µl) was placed,
179 using micropipette, above the sample near the edge closest to the camera. The measurement of
180 the contact angle of the drop is carried out using “*Image J*” software with “*DropSnake*” plug-
181 in for contact angle measurements (Yamauchi, Riko et al. 2005, Ribea, Skov et al. 2016, Chen,
182 Muros-Cobos et al. 2018, Han, Shin et al. 2022).

183 *Preparation of BCac0.4*

184 The Cac0.4 was prepared according to S. Chaouf et al. method (Chaouf et al. 2019, 2020).
185 Briefly, homogenous and transparent cellulosic solution was obtained by dissolving 1 g (6.2
186 mmol AGU) of cellulose in 50 ml of NaOH/Urea aqueous solution (3/2/45, w/w/v), then 1.3 g
187 (18.3 mmol) of acrylamide were added under stirring. The mixture was refluxed at 60 °C for 3
188 h. The Cac0.4 was recovered by precipitation and vacuum filtration. However, the
189 hydrophobization steep of Cac0.4 was carried out using the alkali Williamson reaction in
190 aqueous medium according to I. Jilal et al. method (Jilal et al. 2018a, b; Jilal et al. 2019), where
191 HEC has been replaced by Cac0.4 as water-soluble base polymer to be grafted. 1.8 ml (15
192 mmol) of benzyl bromide was added slowly, at 60 °C, to 1 g (5 mmol AGU) of Cac0.4
193 dissolved in 20 ml of NaOH 1N alkali aqueous solution. The homogenous transparent solution
194 becomes cloudier after 20 min indicating the apparition of the first BCac0.4 hydrophobic
195 particles. After 3 h, the mixture was neutralized using HCl 1N solution, and the precipitated
196 BCac0.4 was recovered, by vacuum filtration and frequently washed with water and dried at 60
197 °C until constant weight then kept in the desiccator for one week with P₂O₅.

198



199

200 **Fig.1.** The Reaction pathway of BCac synthesis

201 *Preparation of EOs-loaded BCac (BCac-Oil)*

202 The system consisting of EOs/BzBr/SDS10% (2/5/1, v/v/v) was stirred for 15 min, where the
 203 micellar system has been involved, and added under stirring to 2 g (10 mmol AGU) of Cac0.4
 204 dissolved in 20 ml of 1N NaOH aqueous solution. The mixture was heated to reflux, with
 205 stirring, for 2 h at 60 °C. BCac-Oil showed a sandy appearance, recovered under vacuum
 206 filtration and washing with water, ethanol then with ether.

207 **Results and discussion**

208 Synthesis and structure characterization of BCac0.4 (FTIR-ATR, ¹H NMR and ¹³C NMR)

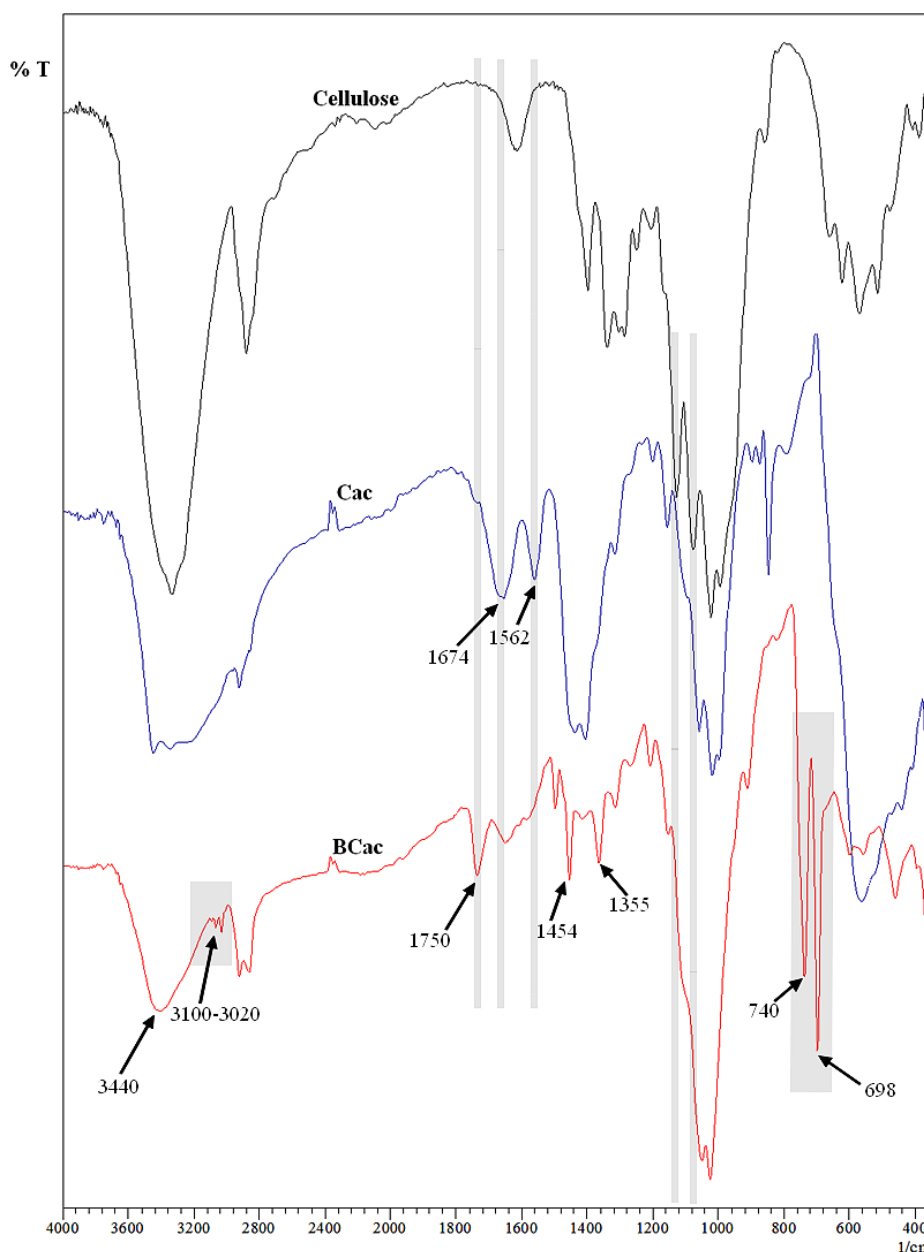
209 The Williamson etherification reaction of cellulose (in aqueous medium) was taken, in this
 210 study, as a model reaction to demonstrate that the Cac0.4 can contribute to solve the major
 211 obstacle of cellulose chemistry, solubility. The repeating unit in cellulose (glucose unit) is
 212 characterized by the constant acid dissociation value (pK_a) of 12.92 (Kortüm et al. 1960;
 213 Kortüm 1961). The same value was theoretically confirmed by Babkin et al. based on the AB
 214 INITIO quantum chemical calculation method, where the acid strength of glucose is assessed,
 215 and it is established that it relates to weak H-acids category (pK_a = 12.7) (Babkin et al. 2012).

216 According to pKa values of AGU and that of NaOH alkali solution, the aqueous alkali
217 alkoxylation of AGUs is strongly suggested by deprotonation of H-alcohols in NaOH solution
218 (Guo and Rockstraw 2007). This allows the occurrence of the Williamson etherification
219 reaction under mild and homogeneous green experimental conditions (Jilal et al. 2018a, b; Jilal
220 et al. 2019, 2021), and thus avoids the use of stronger bases (e.g. NaH, NaNH₂, etc.) as well as
221 the expensive/toxic solvents with very complicated systems and compositions. In this work, the
222 nucleophilic substitution was carried out using the Williamson S_N2 hydrophobization reaction
223 of acrylate water-soluble cellulose (Cac0.4) by benzyl bromide (Fig. 1). First, the Cac0.4 was
224 alkoxyated in NaOH alkali solution to enhance its nucleophilic character and to increase the
225 electron density on the oxygen nucleophile, where the conjugate base (RO⁻, Na⁺) was created
226 by the neutralization of the ROH alcohol acidity by OH⁻, and then the reaction of RO⁻ with
227 an alkyl halide. In addition, the use of equimolar quantity of NaOH (or a slight excess), relative
228 to the functionalizable groups of the AGU, makes it possible to avoid the majority of parasitic
229 side reactions, in particular, the hydroxylation reaction of the alkyl halides.

230 Therefore, this result indicates that the Williamson S_N2 benzylation reaction was successfully
231 carried out under green and homogeneous conditions. In addition, the extreme variation of the
232 contact angle shows that the introduction of the benzyl entities into the cellulosic structure
233 sources shows drastic changes in the surface energy distribution that induce the modification
234 of hydrophilic/hydrophobic behavior of the polymeric surface.

235 FTIR-ATR spectra of unmodified, acrylated (Cac0.4), and benzylated (BCac) cellulose are
236 shown in Fig. 2. The spectrum of unmodified cellulose shows the characteristic absorption
237 bands at 3420, 2940, 1647, 1440, 1388, 1335, 1262, 1169, 1073 and 903 cm⁻¹. The wide
238 absorption band around 3420 cm⁻¹ is attributed to the O–H stretching vibration, and the
239 absorption band at 2940 cm⁻¹ is associated to the C–H stretching vibration (Knop et al. 2011;
240 Chen et al. 2018a, b). Moreover, the absorption bands located at 1440 and 1388 cm⁻¹ are related
241 to the deformation of the O–H plane of the primary alcohol and the C–H symmetric bending
242 vibration in –CHOH– respectively (Arshad et al. 2016), where the band absorption at 1647 cm⁻¹
243 was attributed to natural absorption of water (Johar et al. 2012). Thus, the absorption bands
244 around 1335 cm⁻¹ and 1262 cm⁻¹ are attributed to the characteristic C–C and C–O vibrations of
245 the cellulosic skeleton (Pappas et al. 2002). The peak at 1169 cm⁻¹ was assigned to the
246 asymmetric C–O vibration, while the one at 1073 cm⁻¹ was attributed to the stretching C–O–C
247 vibration of the glucopyranose cycle (El Barkany et al. 2009; Li et al. 2009) while the band at
248 903 cm⁻¹ is a feature of the β-(1,4) glycoside bond (Abdulkhani et al. 2013). In comparison with

249 the cellulose FTIR-ATR spectrum, the Cac0.4 spectrum of the acrylated cellulose, as prepared,
250 showed the appearance of new absorption bands ascribed to the grafted acrylamide group. The
251 appearance of a new broad absorption band at 3223 cm^{-1} attributed to the vibrations of the
252 amide ($-\text{NH}_2$) indicates the success of the acrylamide grafting reaction (Maafi et al. 2010).
253 Moreover, the new peaks detected at 1674 cm^{-1} , 1562 cm^{-1} and 1421 cm^{-1} were attributed to
254 the stretching vibrations of the $\text{C}=\text{O}$ carbonyls of the primary amide, asymmetric and symmetric
255 carboxylate groups, respectively (Fakoya 2013; Krivoshein et al. 2016). Furthermore, the
256 presence of the carboxylate functions on the FTIR-ATR spectra is due to the alkaline nature of
257 the reaction medium which induced the saponification of the grafted amide groups to
258 carboxylate groups. The presence of amide groups can affect the results that impose their total
259 saponification. So, the second step that was devoted to the alkaline saponification of Cac was
260 realized in a alkali solution of NaOH (4 N) for 12 h according to our process published recently
261 by Sara et al. (Chaouf et al. 2020). The disappearance of the characteristic band at around 1647
262 cm^{-1} , attributed to the deformation of water molecules naturally absorbed in the cellulosic
263 structure, is a strong indication of the macromolecular chains separation thus allowing the
264 escape of small molecules trapped in the polymer network. The BCac FTIR-ATR spectrum
265 shows a strong decrease in the intensity of the OH stretching absorption band at around 3440
266 cm^{-1} indicating that they were consumed during the grafting reaction. Moreover, the success of
267 the benzylation reaction in an aqueous medium is also confirmed by the increase in the ratio of
268 stretching vibration intensities between $-\text{CH}-$ and $-\text{CH}_2-$ bonds between 2920 and 2880 cm^{-1}
269 (Garside and Wyeth 2003). The substitution of OH groups by benzyl entities is evidenced by
270 the appearance of new aromatic elongations ($=\text{C}-\text{H}$) vibrations between 3100 and 3020 cm^{-1}
271 and $\text{C}=\text{C}_{\text{sp}2}$ that located at 1454 cm^{-1} (Tatzber et al. 2007; Vickers 2017). The appearance of
272 new absorption bands characterizing the angular deformation (out of plane) of the
273 monosubstituted aromatic $\text{C}-\text{H}$ bands at 740 cm^{-1} , and the aromatic $\text{C}=\text{C}$ angular deformation
274 bands at 698 cm^{-1} (Cullum and Vo-Dinh 2003; Ghorbani Chaboki et al. 2019), indicates that
275 the incorporation of benzyl groups into the polymer structure of Cac0.4 has been successfully
276 achieved. Moreover all characteristic absorption bands of amide function ($-\text{CO}$ and $-\text{NH}_2$), or
277 acrylamide (π bond of $-\text{C}=\text{C}$ at 1614 cm^{-1}), and the benzyl bromide vibration ($\text{C}-\text{Br}$ between
278 600 and 650 cm^{-1}) were not recorded on the BCac FTIR-ATR spectrum indicating that the
279 resulting BCac is free of any residual by-products.



280

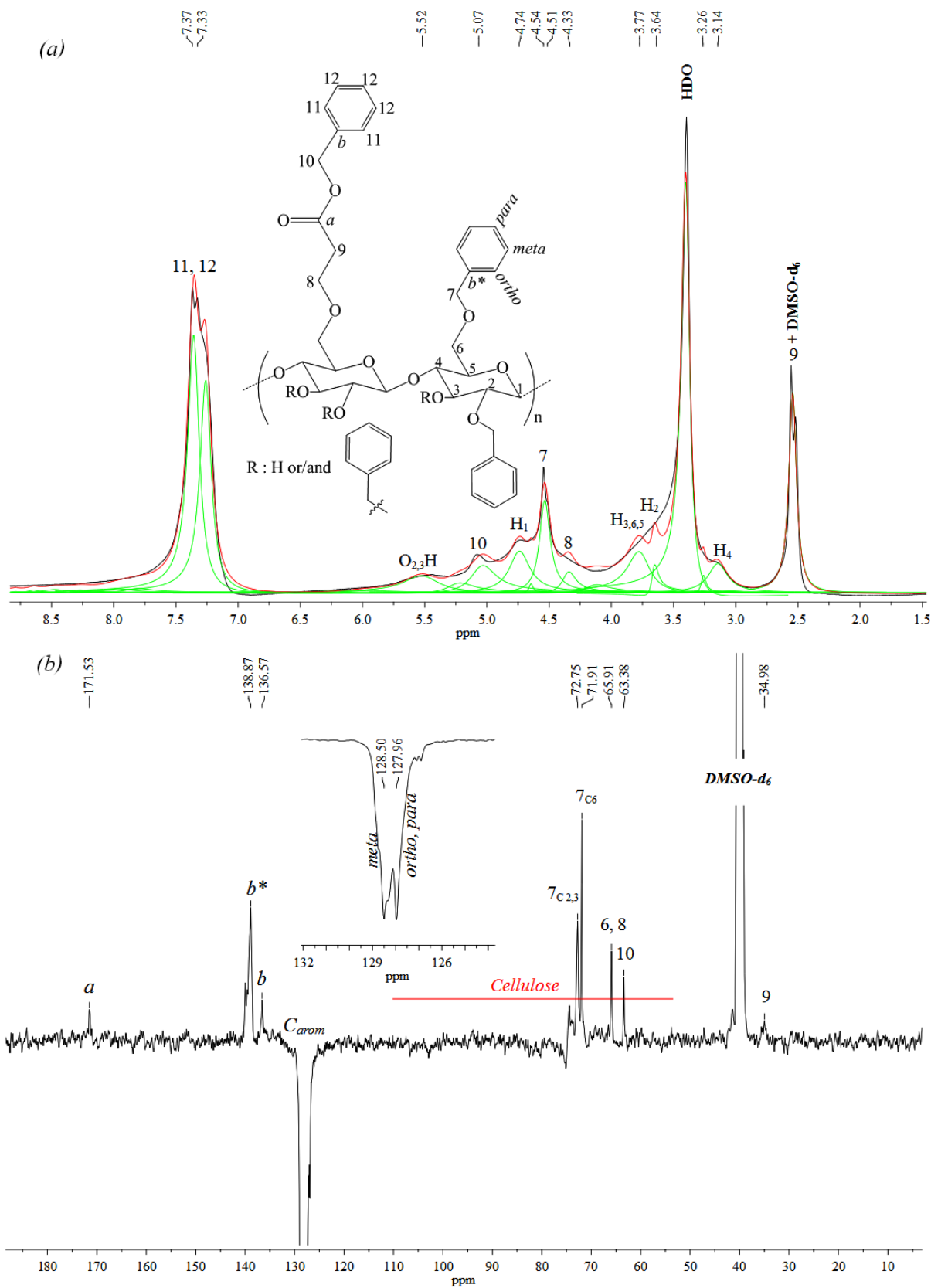
281 **Fig.2.** FTIR-ATR spectra of unmodified cellulose, hydrophilic acrylated cellulose (Cac) and
 282 hydrophobic benzylated Cac (BCac)

283 NMR structural measurements proved to be very useful in the carbohydrate chemistry field
 284 especially in the assignment of the resonance signals of cellulose and cellulose derivatives. The
 285 typical assignment of ¹H-NMR BCac spectrum in DMSO-d₆ is shown in Fig. 3a. The sharp
 286 ring proton signals of the cellulose skeleton (AGU) are shown between the resonances 2.8 and
 287 5.6 ppm, although the AGU protons signals appeared at 3.14, 3.64, 3.77, 4.74 and 5.52 ppm
 288 which are ascribed to H₄, H₂, H_{3,5,6}, and H₁, respectively (El Idrissi et al. 2013; Song et al.
 289 2017). Moreover, the broad signal recorded at 5.52 ppm belongs to the residual hydroxyl
 290 protons linked to the carbons C2 and C3 (–O₂H and –O₃H) (Guo et al. 2012). At the same time,

291 slight shifts of the signal resonances can be encountered compared to the proton resonances of
292 the starting polymers (Cellulose and Cac0.4) (Fig. SD1); this indicates the modification of the
293 nuclear magnetic energy levels and consequently the modification of the environment polymer
294 electronics. Indeed, each recorded chemical shift on an NMR spectrum corresponds to the
295 disturbance of the nuclear resonance frequency within the polymer, where the change in
296 electron density of adjacent atoms (chemical bonds) in the polymeric structure behaves as
297 electronic shielding attenuating the magnetic field exerted on the nuclei.

298 Under the used experimental conditions in this work, including the alkalinity of the medium
299 and the presence of alkoxides and carboxylates as two reactive functions, the two mechanisms
300 of formation of benzyl esters and ethers were highly expected and favoring ether linkage
301 regarding the low DS of acrylates. The resonances of the aromatic protons (11 and 12) are
302 recorded between 7.5 and 7.7 ppm (7.33 and 7.37) ppm (Kim et al. 2018). The strong signal at
303 4.54 ppm and that located at 5.07 ppm are corresponding to the benzyl methylene protons
304 linking to the ether (CH₂—7) and ester (CH₂—10) groups, respectively (Jilal et al. 2018a, b),
305 and the integration ratio value between them is $I_{7/10} = 10.4 = 2.5$. In addition, the acrylate
306 methylene proton resonances at 4.33 (CH₂—8) and 2.55 ppm (CH₂—9) are overlapping by
307 the broader cellulose proton resonances and those of DMSO-d₆, respectively (Brar and Kaur
308 2005).

309



310
 311 **Fig.3.** (a) ^1H NMR and (b) ^{13}C NMR-APT spectra of Benzylated Cellulose Acrylate (BCac, DS_{Bnz} and
 312 $\text{DS}_{\text{Acrl}}0.4$) in DMSO-d_6

313

314 The carbon chemical shift distribution of elaborated BCac polymer was investigated using ^{13}C
315 NMRAPT spectral technique. BCac ^{13}C NMR-APT spectrum has the typical AGU carbon
316 peaks between 60 and 105 ppm (Fig. 3b), and the chemical shifts of six carbons of
317 anhydroglucose residues were slightly different to the unmodified cellulose and that is due to
318 the environmental effect (Jabir et al. 2022). In this field, the chemical shift and signal intensity
319 of cellulosic carbons, in particular the C1 anomeric carbon (providing the gluco-configuration)
320 has been widely discussed in the literature. (Kono et al. 2015). In this regard, Yuxiang Huang
321 et al. have shown, by studying the thermal effect on the supramolecular structure of cellulose,
322 that the chemical shift of C1 can vary between 96 to 108 ppm depending on the polymorph
323 predominance ($\text{I}\alpha$, $\text{I}\beta$ and II) and depending on the temperature treatment. The C1 peak was
324 detected as a sharp singlet for cellulose I and a sharp doublet split for cellulose II (Huang et al.
325 2019). Also, in the case of short cellulosic chains, additional chemical shifts attributed to the
326 C1 ends (C1 α -end and C1 β -end) were recorded around 92.7 and 99 ppm, respectively (King
327 et al. 2018; Yuan et al. 2022). On the other hand, the extensive ^{13}C NMR investigation of
328 cellulose derivatives indicated that the splitting of the C1 signal is attributed to the effect of the
329 molecular environment, in particular the degree of substitution of adjacent C2-hydroxyl and the
330 chemical nature of the grafted entities. Indeed, Yanzhu Guo et al. showed that chemical shifts
331 of C1 carbons adjacent to unsubstituted and substituted C2-hydroxyl groups were detected at
332 103.0 ppm and 99.6 ppm, respectively (Guo et al. 2013). However, the drastic effect of grafted
333 entities and their DS on C1 signal intensity was shown by Pierrick Berruyer et al. where a very
334 weak peak signal intensity of C1 (comparable to background noise) was noticed in the case of
335 modification of C2-OH by hexyldimethylsilyl groups (TDMS), but the strong peak intensity
336 was observed again after substitution with methyl groups (Berruyer et al. 2021). In this paper,
337 the reduction in signal intensity of C1 on the ^{13}C NMR-APT spectrum of BCac (Fig. 4b) was
338 attributed to the modifying effect of the adjacent C2-hydroxyl, where the intensity of C1 was
339 higher in the ^{13}C NMR spectrum of Cac0.4 which indicates free unsubstituted C2-OH in
340 Cac0.4 (Chaouf et al. 2020).

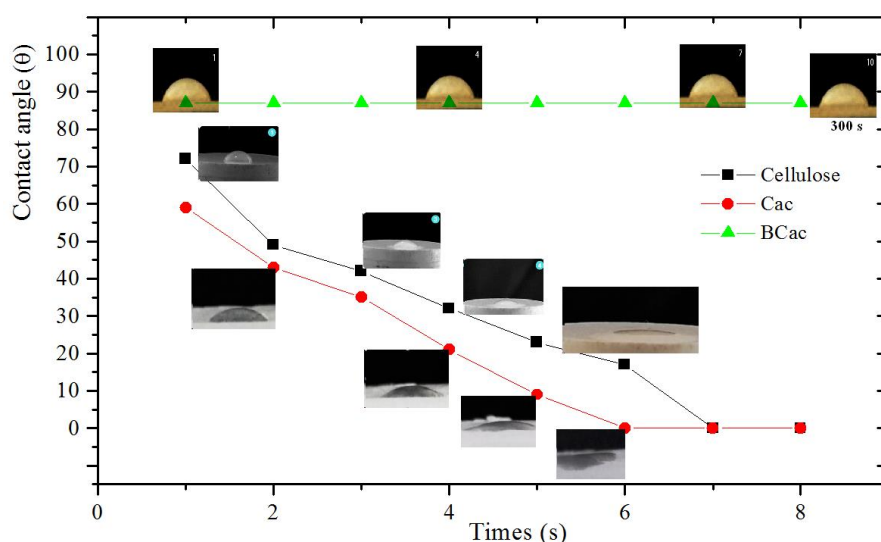
341 Furthermore, the peaks of acrylate entities were established around 35.0 ppm (Cacrylate-9) and
342 65.9 ppm (Cacrylate-8), then the acrylate carbonyl signal was recorded at 171.5 ppm (Cacrylate-a)
343 (Chaouf et al. 2019). However, the absence of the carboxylate carbonyl signal at
344 180 ppm on the BCac ^{13}C NMRAPT spectrum and the deviation of this chemical shift compared
345 to the carboxylate carbonyl, discussed in our previous paper for cellulose acrylate (Cac)
346 (Chaouf et al. 2020), indicates that the benzylation grafting was carried out not only on the

347 alkoxide groups but also affected all the acrylate functions through the creation of ester bridges.
348 The resonances of the substituent entity methylene ($-\text{CH}_2$) carbons (benzyl moieties) in
349 benzylated cellulose acrylate anhydroglucose unities is strongly dependent on AGU
350 nucleophile carbonic position. The chemistry of carbohydrates (cellulose and its derivatives)
351 has a unique feature in terms of the regioselectivity of reaction attack. The partial modification
352 of hydroxyl groups depends on their accessibility and their reactivity, which leads to a
353 difference in chemical shifts for the same attached unit on different positions (C2, C3 and/or
354 C6) AGU. Therefore, the strong indication of the substitution at 3 AGU positions was given by
355 the appearance of nearest distinct resonances distribution at 63.4 ppm, 71.9 ppm and 72.8 ppm,
356 which are attributed to benzyl methylene carbon grafted within acrylate (C-10), position C6 (C-
357 7C6) and positions 2 and 3 (C-72,3), respectively (Qi et al. 2012).

358 The spectra reveal quaternary aromatic carbon peaks of benzyl groups at 136.6 ppm (C-b)
359 (Gong et al. 2017) and at 138.9 ppm (C-b*) which assigned to the ether linkage associated to
360 the Williamson SN2 grafting (Huang et al. 2020). Additionally, the significant resonance peaks
361 at around 127–129 ppm are assigned to sp² aromatic carbons (C-11 and C-12) (Jilal et al. 2018a,
362 b). The inversion of the orientation in the ¹³C NMR-APT spectrum provides additional
363 information that indicates the presence of sp²-carbon character in the fine structure of BCac.
364 The degree of substitution DS-value of grafted benzyl entities and their distribution on the AGU
365 carbons can be determined using the peak integration intensities in the ¹H-NMR spectra
366 according to the above peak assignments. The integration value of the acrylate proton signal
367 (corresponding to DS value of 0.4 of Cac0.4) and NMR results indicate that all C6 hydroxides
368 have completely reacted (disappearance of C6 carbon resonance at around 60 ppm). Thus, the
369 partial and total DS values were evaluated as: $DS_{\text{benzyl propanoate cellulose}} (\text{R1}) = 0.4$, $DS_{\text{benzyl cellulose}}$
370 $(\text{R2}) = 1.0$ and $DS_{\text{benzyl propanoate cellulose}} = 1.4$.

371 *Contact angle characterization*

372 The contact angles of unmodified cellulose, Cac0.4 and Benzylated cellulose (BCac) with water
373 were investigated to study the effect of the acrylation and the benzylation of cellulose on the
374 surface hydrophilic character (Fig. 4). Contact angle reduced to around 15° due to the acrylation
375 of cellulose, indicating the improved hydrophilicity. While no change of contact angle (around
376 90°) was observed in BCac, this phenomenon demonstrated an excellent hydrophobicity.



377

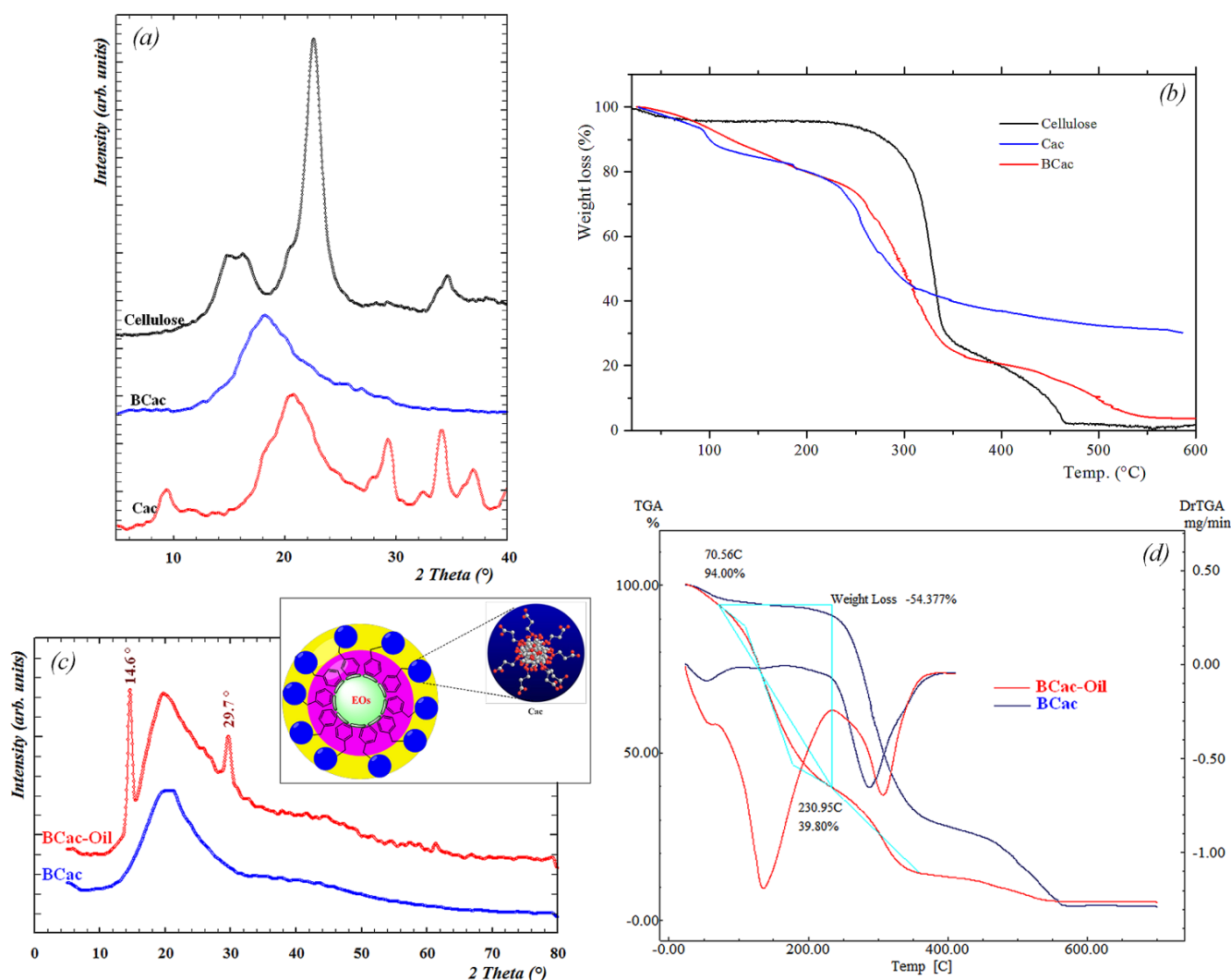
378 **Fig.4.** Contact angle versus. Time of unmodified cellulose, hydrophilic cellulose-acrylate (Cac) and
 379 benzylated Cac (BCac)

380 *X-ray diffraction characterization*

381 The X-ray diffraction (XRD) patterns of unmodified cellulose, Cac0.4 and BCac were shown
 382 in Fig. 5a. The XRD patterns demonstrate severe produced changes of the crystalline order
 383 caused by the introduction of the acrylate and the benzyl entities in the cellulosic structure.
 384 First, the acrylation of the cellulose reveals the complete destruction of cellulosic Miller planes
 385 (hkl) 1–10, 110, 200 and 004 corresponding to the Bragg 2θ angles 15.0° , 16.3° , 22.6° and 34.5°
 386 respectively, which characterize the cellulose I allomorph (Lu et al. 2015). In addition, no effect
 387 of the alkali reaction conditions was perceived on the polymorphism transition (Carrillo-Varela
 388 et al. 2018), and the new peaks that appeared in the Cac0.4 diffractogram may be suggested the
 389 new supramolecular physical interactions that generated from the interactions between the
 390 protons and the carboxylate group ions.

391 The Williamson SN_2 reaction in this work strongly affected the crystalline compartment of the
 392 benzylated cellulose acrylate (BCac), where the amorphous aspect becomes more established
 393 for BCac than the unmodified cellulose and cellulose acrylate samples. After the encapsulation
 394 of the EOs in BCac (BCac-Oil), new crystalline material was characterized by the appearance
 395 of two diffraction peaks at 2θ values of 14.6° and 29.7° (Fig. 5c). These results indicate that the
 396 Rosemary essential oil was successively loaded in the biodegradable BCac polymer as plastic
 397 coacervates. Furthermore, and from the periodicity perspective, the achieved results in this
 398 paper were in opposition to those reported in some previous papers, where the benzylated

399 cellulose samples were highly ordered and very well diffracted diffractograms were found
 400 (Isogai et al. 1993; Saliu et al. 2017).



402 **Fig. 5.** a) x-ray diffractograms and b) thermograms (TGA) of unmodified cellulose, hydrophilic
 403 cellulose-acrylate (Cac) and benzylated Cac (BCac), c) x-ray diffractograms and d) thermograms (TGA)
 404 of benzylated Cac (BCac) and EOs loaded BCac (BCac-Oil)

405 *Thermal characterization (TGA/DrTGA)*

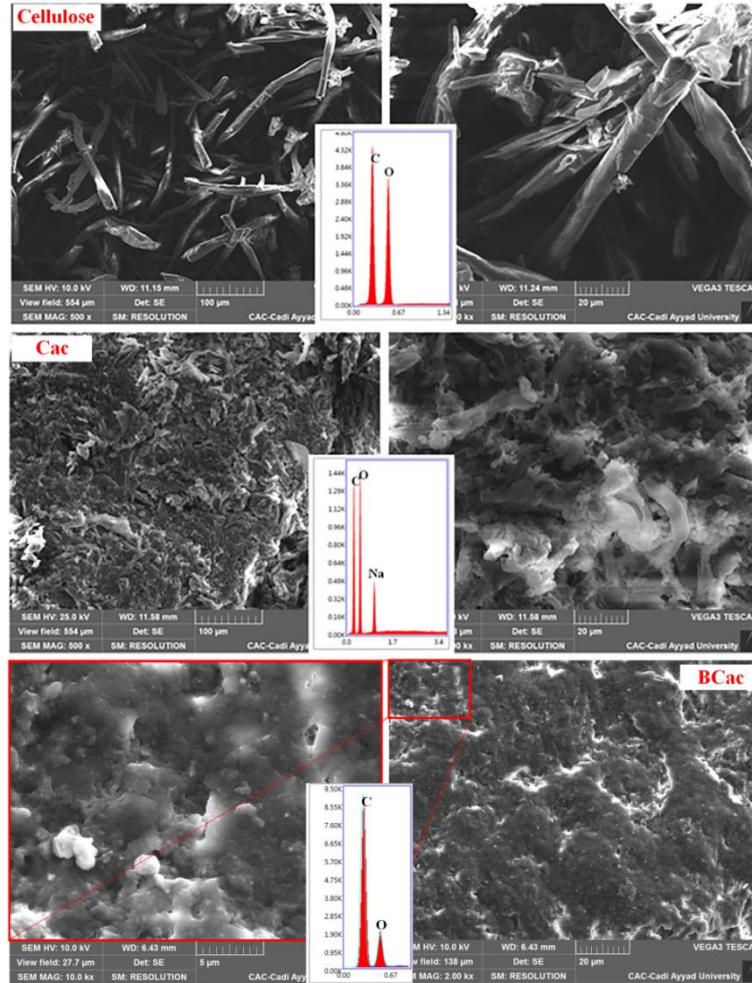
406 The effect of the acrylation reaction of the cellulose in an aqueous-alkali-urea solution on the
 407 thermal behavior was largely discussed in our previous paper (Chaouf et al. 2020). In brief, the
 408 thermal decomposition behavior of both starting polymers, unmodified cellulose and Cac0.4,
 409 showed two weight loss stages, corresponding to the endothermic evaporation of the retained
 410 moisture at around 100 °C, where the second major exothermic weight losses were assigned to
 411 the thermal decomposition of cellulose backbone and the grafted groups. Additionally, Sarah
 412 et al. found that the second decomposition was accompanied by two exothermic peaks (335 °C

413 and 461 °C) attributed to the decomposition of the amorphous and crystalline parts (Calahorra
414 et al. 1989; Chaouf et al. 2020). Yet, a slight loss of thermal stability was recorded for Cac0.4
415 (208 °C) compared to unmodified cellulose (252 °C), which is due to the significant decrease
416 in structural cohesion density produced by acrylate grafting and the intercalation of polymer
417 chains of cellulose. However, the benzylation of Cac removed the ionic forms in the polymeric
418 structure and is replaced by the aromatic sites which provide important hydrophobic
419 interactions to slightly increase the thermal stability of BCac at around 240–250 °C (Fig. 5b).
420 Furthermore, the weight of residues over 450 °C is pertinent thermal information confirming
421 that the SN2 Williamson benzylation of acrylated cellulose was successfully achieved in the
422 aqueous medium. While the weight loss above 450 °C showed a stable value around 30% of
423 residual weight for Cac0.4 which interprets the existence of the grafted sodium carboxylate
424 ionic form (Yan et al. 2009), therefore, this value has become negligible on the BCac
425 thermogram indicating the successful incorporation of benzyl species into the cellulosic
426 structure through low DS acrylate as a cellulose derivative and intermediate polymer. On the
427 other hand, the EOs loaded BCac (BCac-Oil) thermogram show a high degree of the thermal
428 behavior similarity to that of BCac at the temperatures above 230 °C (Fig. 5c), which designates
429 the degradation phase of the BCac enveloped Rosemary EOs. Moreover, the first endothermic
430 recorded on the BCac-Oil thermogram between room temperature and 100 °C revealed that the
431 plastic coacervates contain at around 6%w of moisture and interfacial adsorbed oil. Since,
432 Benzylcellulose is known as a good Oil absorber, which is ensured by hydrophobic forces, the
433 release of EOs trapped in the particle core may require more energy cost than that equivalent to
434 the elimination of water molecules adsorbed on the surface of the particles (Saliu et al. 2017).
435 The new dramatic weight loss on the thermogram of BCac-Oil was recorded over the
436 temperature range of 100 to 230 °C, which is attributed to the evaporation of the internal EOs
437 in microparticles that escape (~ 54%w loaded) under the action of the thermal pressure
438 manifesting the thermal release of the oily molecules.

439 *Morphology characterization (SEM/EDX)*

440 Besides, Scanning Electron Microscopy (SEM) has been widely exploited as an effective and
441 useful technique to assess morphological changes against different physical or chemical
442 treatments of materials. The cellulosic materials and their derivatives often show radical
443 microstructural modifications (Ghorbani et al. 2018). The microstructural analyses of cellulose,
444 cellulose acrylate (Cac0.4) and benzyl cellulose acrylate (BCac) are shown in the Fig. 6, SEM
445 images of Cac0.4 show a strong effect of the acrylate substitution even at low DS on the

446 cellulosic microfibrillar morphology degradation, where the resulted microstructure of Cac0.4
447 proved the modification of the supramolecular interactions indicating the reduction of the H-
448 bond density that awarded to the polymer new physicochemical properties, especially the water
449 solubility. The incorporation of benzyl entities in the BCac designated a more compact matrix
450 and dense microstructure appearance compared to that of Cac0.4 and the complete
451 disappearance of the microfibrillar cellulosic character suggesting the predominance of the
452 hydrophobic force interactions against the H-bond ones. A slight increase in the atom ratio of
453 O/C and the appearance of Na both indicated the successful saponification of Cac0.4 in EDX
454 spectra. Moreover, the elemental profile of benzylated cellulose acrylate (BCac) was studied
455 according to the recorded EDX spectrum (Fig. 6), which shows a strong decrease of the atomic
456 ratio (O/C) indicating a high value of carbon countenance that warns from the grafted benzylic
457 entities. In addition, the disappearance of the Na peak on BCac EDX pattern is an alternative
458 solid indication of the occurrence of the benzylation grafting reaction on the carboxylate sites
459 in addition to the alkoxylated hydroxyl groups. The grafting of benzylic groups explains the
460 stability of the hydrophobic aspect where the total elimination of the hydrophilic character
461 coming from the ionic bond between carboxylate and Na ion on the one hand, and the
462 substitution of the mobile hydrogen by the hydrophobic aromatic sites on the other hand.



463

464 **Fig. 6.** SEM images and EDX spectra of unmodified, cellulose acrylated (Cac0.4) and hydrophobic
 465 benzylated Cac (BCac0.4)

466 **Flory-Huggins Thermodynamics Theory and Application**

467 According to the Hansen solubility parameter (HSP) theory (Hansen 1967), the energy of
 468 vaporization can be divided into non-polar (dispersive, d) and polar (p) forces and hydrogen-
 469 bonding (h) contributions (Eq. 1). Moreover, the basic solubility parameter concept, correlating
 470 between the cohesive energy density (CED) and mutual solubility, allows the expression of the
 471 Hildebrand solubility parameter (δ_t) in terms of the three HSP (δ_d , δ_p , δ_h) related to each
 472 contribution (Eq. 2) (Breitkreutz 1998). The corresponding equation for the mixing enthalpy
 473 (ΔH_m) can be calculated using the Eq. 3, where the δ_1 and δ_2 are solubility parameters of
 474 solvent and polymer, respectively (Krevelen and Nijenhuis 2009).

475
$$\Delta E_v = \Delta E_{coh} = \Delta E_d + \Delta E_p + \Delta E_h \quad (1)$$

476
$$\delta_t^2 = \delta_d^2 + \delta_p^2 + \delta_h^2 \quad (2)$$

$$477 \quad \Delta H_m = \phi_1 \phi_2 \left[(\delta_{d1} - \delta_{d2})^2 + (\delta_{p1} - \delta_{p2})^2 + (\delta_{h1} - \delta_{h2})^2 \right] \quad (3)$$

478 On the other hand, according to the regular solution theory, the relationship between the Flory–
 479 Huggins interaction parameter (that quantifies the enthalpic value of mixing in polymer–solvent
 480 system) and the solubility parameters was shown in the Eq. 4 (Lindvig et al. 2001). However,
 481 the “1/4” scale factor was intended to make the “volume of solubility” approximately spherical
 482 (Barton 2017). This factor was theoretically predicted by Prigogine et al. to estimate the
 483 solubility behavior of dissimilar molecule mixtures (Prigogine et al. 1957). Furthermore, the
 484 Hildebrand parameters cannot be calculated directly for polymers from heat of vaporization
 485 data because of their no-volatility. However, it is calculated using the indirect correlation or
 486 atomic contribution group method, based on the assumption of different functional groups
 487 contribution (Ravindra et al. 1998). The Van Krevelen and Hoftyzer method (VKH)
 488 calculations were largely used basing on the tables of group values giving the molar volumes
 489 and molar attraction constants of the repeating unit (Krevelen 1972; Van Krevelen 1972).

490 In this work, the Flory–Huggins model was investigated to predict the demixation behavior of
 491 the polymeric cellulose solution during the grafting reaction on the cellulose linear chain, which
 492 can be generalized for other grafting reactions. In this regard, the Flory–Huggins solvent
 493 polymer interaction parameter (χ_{12}) was calculated, for the different degrees of substitution,
 494 using Hansen’s partial solubility parameters (HSP). The Van Kerevlen’s Group Contribution
 495 Method (GCM) was used to determine the HSPs (Eqs. 5–7) according to the changes caused by
 496 chemical modification within the chemical structure of the polymer (Abderahmane et al. 2011;
 497 Jilal et al. 2018a, b), and the results are summarized in the tables SD2 and SD3. F_{di} and F_{pi} are
 498 respectively the molar forces of attraction of the dispersion component and the polar component
 499 (F_p). E_{hi} is the hydrogen bond energy and $\Sigma V_i = V_{m2}$ is the molar volume of the molecule.

$$500 \quad \chi_{12} = \alpha \frac{V_{m1}}{RT} \left[(\delta_{d1} - \delta_{d2})^2 + \frac{1}{4} (\delta_{p1} - \delta_{p2})^2 + \frac{1}{4} (\delta_{h1} - \delta_{h2})^2 \right] \quad (4)$$

501 where α is the correction factor and is equal to the unity value in the absence of polarity
 502 interactions and hydrogen bonds, while it approaches the value 0.5 in the opposite case where
 503 the predominance of physical interactions including polarity and bonds hydrogen. d , p and h
 504 are partial Hansen solubility parameters attributed to the dispersive, polarity and hydrogen
 505 bonds contribution, respectively.

$$506 \quad \delta_d = \frac{\sum F_{di}}{\sum V_i} \quad (5)$$

$$507 \quad \delta_p = \frac{\sqrt{\sum F_{pi}^2}}{\sum V_i} \quad (6)$$

$$508 \quad \delta_h = \frac{\sqrt{\sum F_{hi}}}{\sum V_i} \quad (7)$$

509 The hydrophobization reaction generates a drastic modification of the physicochemical
 510 properties of the cellulose polymers, in particular the water-solubility behavior. This
 511 modification can be explained by the variation of the interactional energy quantities exchanged
 512 between the solvent and the polymer during the reaction. At this point, the interaction parameter
 513 Chi (χ) should be a mathematical function that describes the degree of hydrophobicity of the
 514 cellulosic polymer. Thus, the rate of reaction progress is represented by the degree of
 515 substitution (DS) that is framed between the value 0 and the functionality of the polymeric
 516 segment (δ), and which presents the variable in the function $\chi(\delta)$. In addition, the chemical
 517 modification of repetitive entities within the polymer chain strongly influences the
 518 supramolecular and polymer-solvent interactions, and therefore, a large modification of the
 519 polymeric architecture is expected and results from the structural expansion of the latter. Then,
 520 this geometric modification disturbs the dimensional stability of the Flory network
 521 (thermodynamic boxes), and thus causes modifications in the volume fractions 1 and 2 . In the
 522 present work, the proposed correction at the geometric fluctuation level is to highlight the
 523 variability of the molar volume of the polymer, during the reaction, as a function of DS $V_{m2}(\delta)$
 524) - , and consequently $\phi_1(\delta)$ and $\phi_2(\delta)$. Therefore, the Gibbs free energy of mixing, for a
 525 binary system consisting of n_1 solvent molecules and N_2 polymer chains with an average degree
 526 of polymerization x , is given by the following equation (Eq. 8):

$$527 \quad \Delta G_{mix} = RTN(\delta)[\phi_1(\delta) \ln \phi_1(\delta) \\ 528 \quad \quad \quad + (\phi_2(\delta)/x) \ln \phi_2(\delta) + \phi_1(\delta)\phi_2(\delta)\chi_{12}(\delta)] \quad (8)$$

529 Where,

$$530 \quad \phi_1(\delta) = \frac{n_1 V_{m1}}{n_1 V_{m1} + x N_2 V_{m2}(\delta)} \rightarrow \frac{1}{\phi_1(\delta)} = 1 + \frac{x N_2}{n_1} \beta(\delta)$$

$$531 \quad \phi_2(\delta) = \frac{xN_2V_{m2}(\delta)}{n_1V_{m1} + xN_2V_{m2}(\delta)} \rightarrow \frac{1}{\phi_2(\delta)} = 1 + \frac{n_1}{xN_2\beta(\delta)}$$

$$532 \quad N(\delta) = \frac{V_1}{V_{m1}} + xN_2 \frac{V_{m2}(\delta)}{V_{m1}} = n_1 + xN_2\beta(\delta)$$

533 V_{m1} and V_{m2} are the molar volumes of the solvent and polymer segments, respectively. $N(\delta)$ is
534 the total number of lattice thermodynamic cells normalized to the solvent cell, and $\beta(\delta) =$
535 $V_{m2}(\delta)/V_{m1}$ is the Flory size constant correction that indicate the number of solvent molecules
536 replaceable by a freely orienting segment of the polymer chain, depending on the δ . This
537 expression (Eq. 8) becomes similar to the classical expression if the equal-sized molecules and
538 one segment-polymer conditions are verified. In the case of grafting of functional units on
539 polyfunctional linear polymeric supports (i.e. cellulose), the hypothetical spatial network
540 architecture strongly depends, as the grafting reaction progresses, on the chemical nature of the
541 grafted group, which governs the qualitative aspect of the solvent-polymer and supramolecular
542 interactions. Then, the quantitative representation and the density of the interactions are
543 controlled by the degree of substitution represented symbolically by the functionality of the
544 linear polymer. So it is imperative to determine the expression of $V_{m2}(\delta)$, and taking into
545 account the notion of additivity of volumes, $V_{m2}(\delta)$ can be written in the following form (Eq.
546 9):

$$547 \quad V_{m2}(\delta) = V_{m2}(0) + V_i\delta + V^E(\delta) \quad (9)$$

548 Where, $V_{m2}(0)$ is the molar volume of the polymer before modification ($\delta = 0$), V_i is the molar
549 volume of grafted group and V^E is the excess molar volume of polymer which indicates the
550 effect of grafting reaction on polymer expansion (or contraction), and the expansion (or
551 contraction) coefficient is given as $\delta(\partial V^E/\partial\delta)$ is a constant value. Then the Equation Eq.-9
552 becomes:

$$553 \quad V_{m2}(\delta) = V_{m2}(0) + \delta \left(V_i + \frac{\partial V^E}{\partial\delta} \right) \quad (10)$$

$$554 \quad \rightarrow \beta(\delta) = V_{m2}(\delta)/V_{m1}$$

$$555 \quad = \frac{V_{m2}(0)}{V_{m1}} + \delta \frac{\left(V_i + \frac{\partial V^E}{\partial\delta} \right)}{V_{m1}}$$

$$556 \quad \text{Posing } V_{m2}(0)/V_{m1} = y \text{ and } \left(V_i + \frac{\partial V^E}{\partial\delta} \right)/V_{m1} = z \quad \rightarrow \beta(\delta) = y + \delta z$$

557 Where,

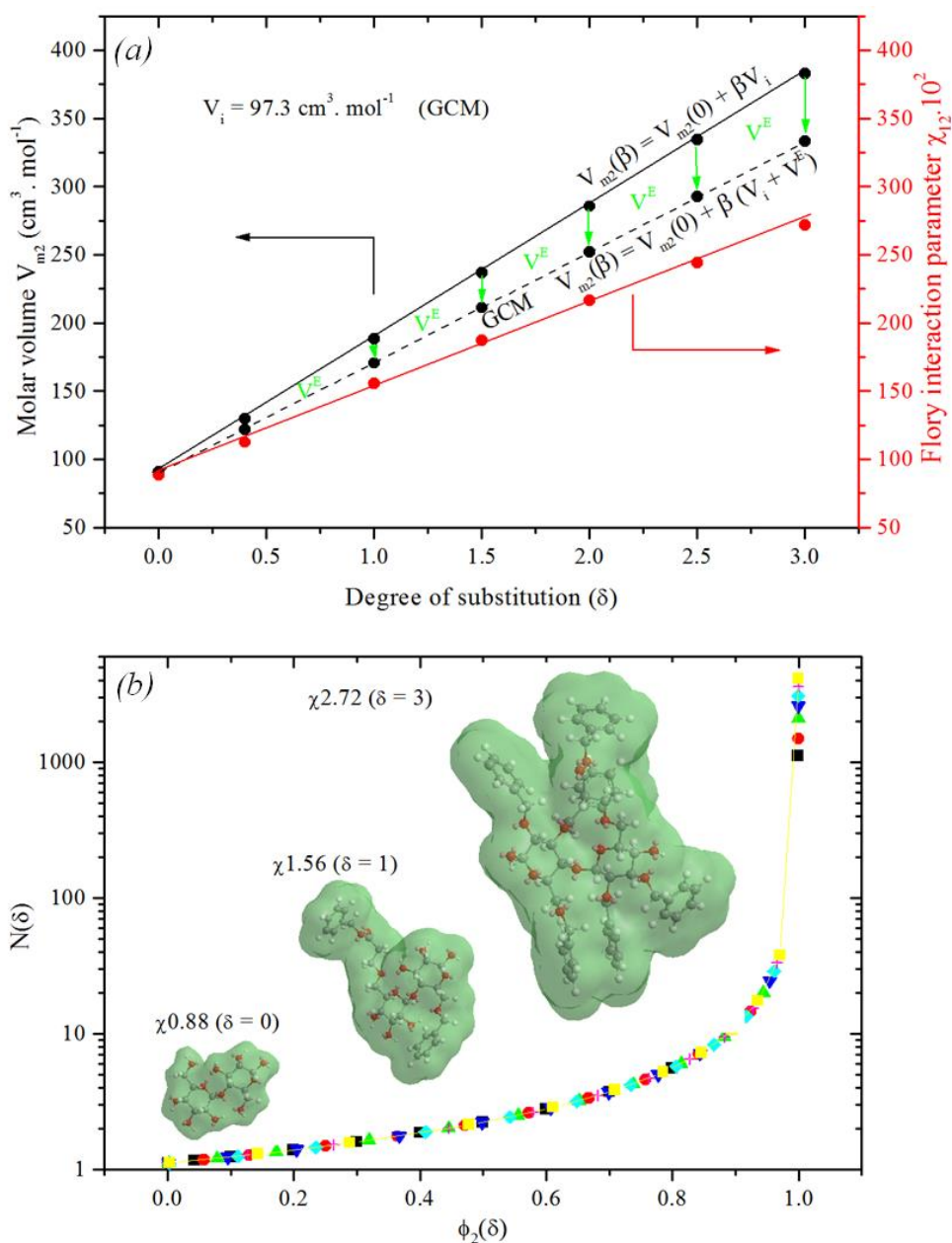
558
$$\frac{1}{\phi_1(\delta)} = 1 + \frac{xN_2}{n_1} \beta(\delta) \quad \rightarrow \quad \frac{1}{\phi_1(\delta)} = 1 + \frac{xyN_2}{n_1} + \frac{xzN_2}{n_1} \delta \quad (11)$$

559
$$\frac{1}{\phi_2(\delta)} = 1 + \frac{n_1}{xN_2\beta(\delta)} \quad \rightarrow \quad \frac{1}{\phi_2(\delta)} = 1 + \frac{n_1}{xyN_2+xzN_2\delta} \quad (12)$$

560
$$N(\delta) = n_1 + xyN_2 + xzN_2\delta = \frac{n_1}{\phi_1(\delta)} \quad (13)$$

561 Under conservative conditions of the physical system where the number of polymeric chains
562 (N_2), degree of polymerization (x), quantity and quality of solvent (n_1), y and z are constants,
563 the benzylation of cellulose acrylate showed a negative expansion factor $\delta(\partial V^E / \partial \delta) < 0$ (Fig.
564 7a), which indicates that the introduction of benzyl species (at a defined value of the degree of
565 substitution) causes a structural contraction of BCac0.4 in comparison to the results obtained
566 from volume additivity reflection. According to the Equation Eq.-12, the substitution of the
567 mobile protons (alcohol and carboxylic acid or carboxylate) of the cellulose acrylate by the
568 benzyl groups drastically modifies the molar volume of the polymeric chain $V_{m2}(\delta)$, and
569 consequently the Flory size-constant correction $\beta(\delta)$ is no longer constant.

570 During the benzylation of cellulose acrylate (Cac 0.4), the total number of constitutional
571 cavities of the thermodynamic network increases by adding the volume occupation of the
572 grafted entities (Fig. 7b). The deviation of total network cell disturbs strongly the fraction values
573 and explains their values displacement. Figure 8 highlights the hypothetical lattice dimensional
574 instability of the polymeric system, where the volume fractions ϕ_1 and ϕ_2 are strongly
575 influenced. The study of the variation of the volume fraction of BCac0.4 ($\Delta\phi_2$), versus its initial
576 volume fraction (Cac0.4) and the degree of substitution (δ), showed that the fractional transition
577 reaches its maximum at the initial fraction of 0.3 and a degree of substitution $\delta = 3$.

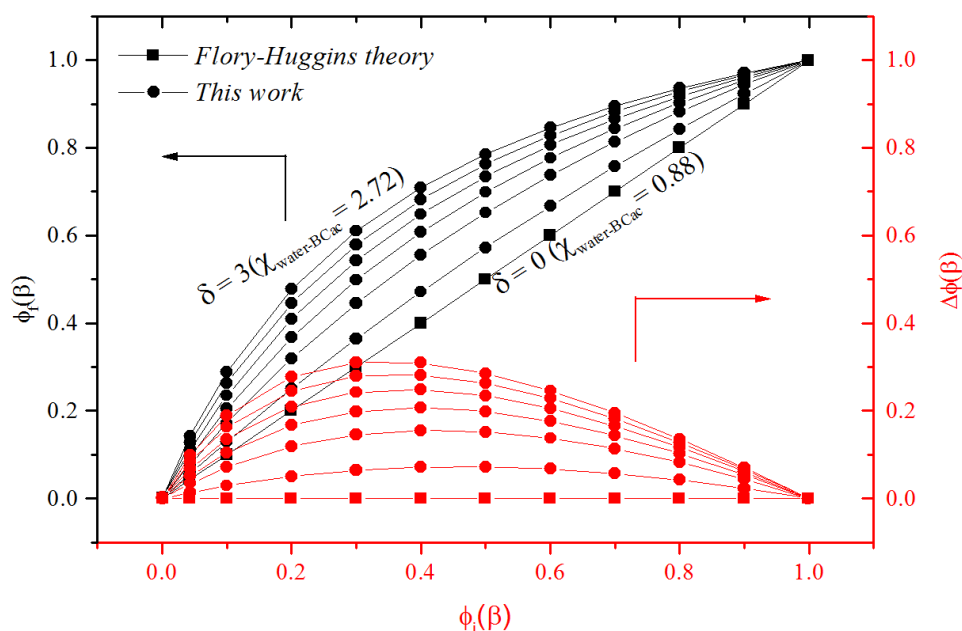


578

579 **Figure 7:** a) Effect of the chemical modification on the excess molar volume of Bcac0.4 and Flory-
 580 Huggins interaction parameter BCac-water (χ_{12}), and b) Effect of the benzylation reaction of Cac0.4 on
 581 the total number of lattice thermodynamic cells $N(\delta)$

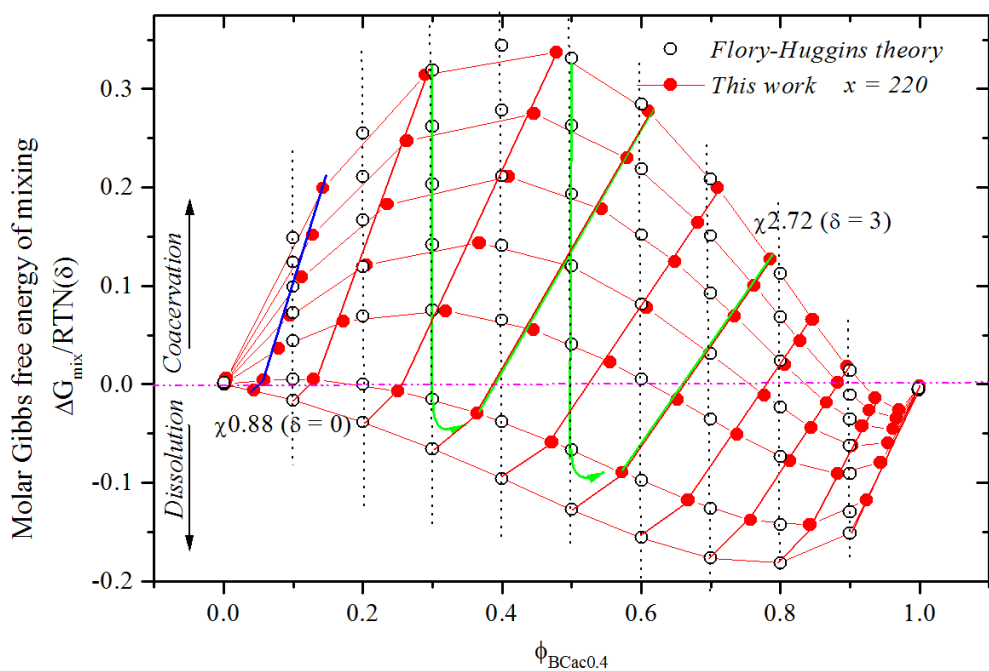
582 In addition, the fractional displacement during grafting onto polyfunctional polymers such as
 583 cellulose causes broad variations in dimensional stability, and these signify the profound
 584 changes in supramolecular interactions, which govern the hydrophilic behavior conversion
 585 boundaries to the hydrophobicity. Then, the expected results based on Flory's theory, where
 586 the hypothesis of thermodynamic network dimensional stability is considered (green lines in
 587 Fig. 9), are largely separated from those determined in this work by applying the fractional

588 displacement approach. Furthermore, taking for example the state of coordinates ($\phi_2 = 0.5$, $\phi_1 = 0.5$), according to Flory $\Delta G_{\text{mix}}/RTN(\delta) > 0$ which indicates the mixture demixation, while the thermodynamic stability of mixing is strongly favored by fractional shift where $\Delta G_{\text{mix}}/RTN(\delta) < 0$ (Fig. 9). Often, the demixation in the absence of modification reactions (χ is constant) is produced by the fractional effect. However, with increasing polymer fraction, two stable mixing zones are expected and favored by negative molar Gibbs free energy values ($\Delta G_{\text{mix}}/RTN(\delta) < 0$); the first was characterized by a high concentration of liquid (solvent) while the other is the solvation of liquid in the polymeric matrix considered as solvent of small solvent molecules. The range of intermediate polymer fractions causes biphasic demixing where the polymer phase is completely separated from the solvent phase ($\Delta G_{\text{mix}}/RTN(\delta) > 0$).



598

599 **Fig.8.** Effect of the benzylation reaction of Cac0.4 on the volume fraction of polymer (ϕ_2)



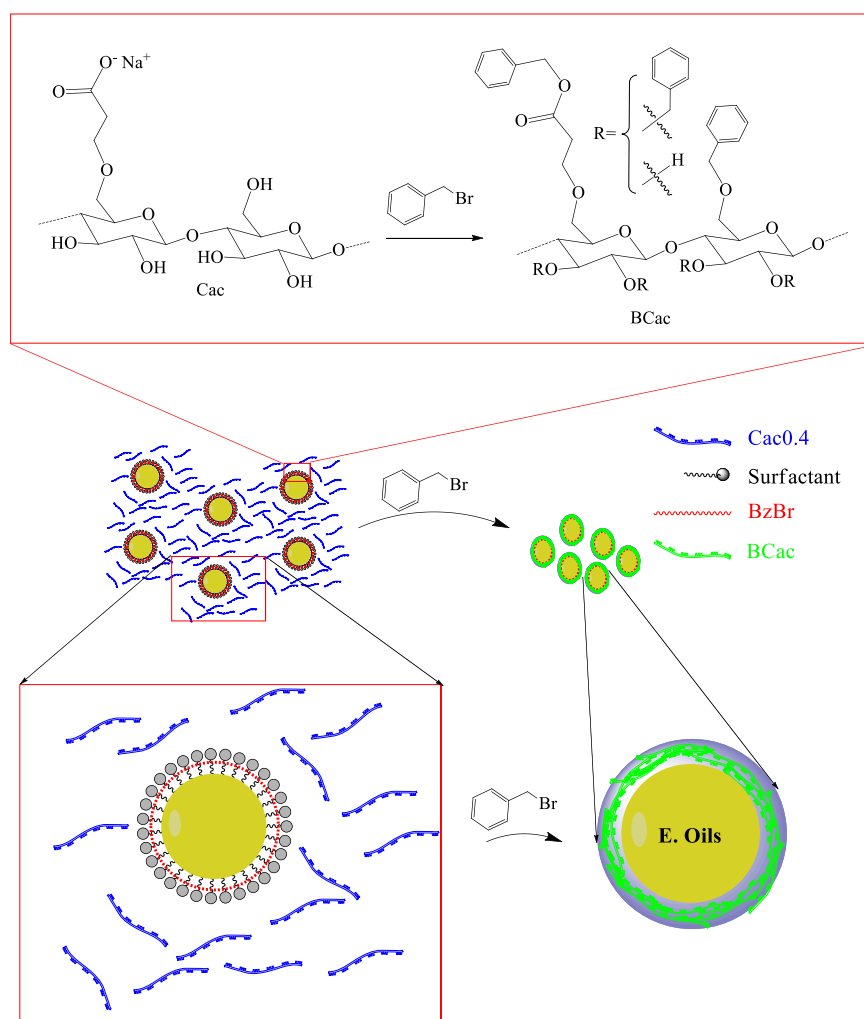
600

601 **Fig.9.** The variation of molar Gibbs free energy of mixing ($\Delta G_{\text{mix}}/RTN(\delta)$) vs. volume fraction of
 602 BCca0.4 in water (ϕ_2) and Flory interaction parameter ($\chi_{\text{BCac-water}}$)

603 In this paper, a novel strategy was investigated for the encapsulation of oils and drugs using a
 604 novel Flory–Huggins thermodynamic approach, where the demixation and the coacervates
 605 formation were favored by increasing the Flory interaction parameter by the modification of
 606 hydrophobic level of polymeric chains upon the reaction. At this point, the free Gibbs energy
 607 of the mixture becomes positive, and the parameters that govern the coacervation phenomenon
 608 are the interaction parameter of Flory (enthalpic magnitude) and fractional shift (entropic
 609 magnitude). Moreover, no changes have occurred about the polymerization degree, and all other
 610 thermodynamic parameters remain constant in the system ($\phi_{1i}, \phi_{2i}, n_1, N_2, x, y, z$). In this
 611 study, an anionic surfactant (SDS) that is represented by a blue line in Fig. 9) was used to form
 612 oily micellar colonies trapping the hydrophobic entities (benzyl bromide) to graft onto Cac0.4
 613 dissolved in aqueous alkali solution (NaOH 1N) ($\Delta G_{\text{mix}} = -18.37 \text{JK}^{-1} \text{mol}^{-1}$). The cellulose
 614 hydrophobization was carried out at the micellar interface, where the DS increases with reaction
 615 time as the hydrophobicity rate of Cac0.4 increases, and then the demixation appears.
 616 According to the thermodynamic study (Fig. 9), the demixation can be obtained even at low DS
 617 (e.g. = 0.4 $\rightarrow \Delta G_{\text{mix}} = +12.79 \text{JK}^{-1} \text{mol}^{-1}$) giving the variation of the mixture Gibbs energy
 618 obtained based on the Flory–Huggins theory results.

619 Increasing the hydrophobic character of the BCac0.4, during the reaction, increases the affinity
 620 of BCac0.4 to the hydrophobic medium, and then the BCac0.4 moved to the micellar surface,

621 and consequently enveloped the oily phase. Moreover, although the BCac0.4 formation is
 622 spectacular elsewhere in the Eos droplets, its migration to the surface of the Eos droplets is
 623 governed by the diffusion under the action of the hydrophobic forces that caused by cellulose
 624 acrylate benzylation (Fig. 10). On the other hand, the NaBr salt, resulting from the Williamson
 625 SN_2 etherification reaction, strongly contributes to modifying the physicochemical properties
 626 of the reaction system, in particular the increase in the critical micellar concentration (CMC).
 627 Thus, it promotes the release of surfactant and its diffusion towards the reaction medium than
 628 it's elimination by washing. So, the rosemary oil coacervates were elaborated upon
 629 modification of the hydrophilic aspect of cellulose (Cac0.4). In this reaction system assuming
 630 that the benzylation reaction is homogeneous in all points of the reaction system [$xN_2 = 10^{-2}$
 631 mol, $n_1 = 1.11$ mol, $x = 220$, $M(Cac0.4) = M_{AGU} + 0.4 * M_{acrylate-Na} = 162 + 0.4 * 95 = 200$
 632 $g \cdot mol^{-1}$].



633

634 **Fig. 10.** BCac0.4 rosemary oil-coacervates formation upon modification of the hydrophilic aspect of
 635 cellulose (Cac0.4)

636 **Conclusion**

637 In this work, the Williamson SN_2 synthesis of BCac ($\text{DS}_{\text{Bnz}} \sim 1.4$) was successively carried out
638 in aqueous alkaline system as the dispersing medium. The difference of pKa values between
639 the mobile acid protons of water-soluble cellulose acrylate (AGU) and the alkali solution
640 (NaOH) leads to the formation of alkoxides, which are more likely to attack the electrophilic
641 centers of the alkyl halide. The proposed chemical structures were confirmed by the recorded
642 results on the vibrational (FTIR-ATR) and nuclear resonance (^1H NMR and ^{13}C NMR-APT)
643 spectra of unmodified, acrylate cellulose (Cac0.4) and benzylated cellulose acrylate (B_{Cac} ,
644 $\text{DS}_{\text{Bnz}} \sim 1.4$ and $\text{DS}_{\text{Ac}} \sim 0.4$). According to X-ray diffraction patterns, the proton substitution
645 by hydrophobic benzyl sites modified the supramolecular interactions and established the
646 drastic changes in the crystalline profile. In addition, the contact angle results showed the
647 extreme modifications of the Cac0.4 hydrophilic to B_{Cac} hydrophobic character, where the
648 contact angle increased from 15° to 90° , respectively. On the other hand, the structural results
649 were in good agreement with the elemental profiles that showed on EDX-spectra. Also, the
650 SEM-images indicated that the microstructure was greatly affected by the Williamson SN_2
651 benzylation of Cac0.4, where the cellulose fibrous morphology was completely destroyed
652 indicating that the Williamson hydrophobization reaction was carried out with success. The
653 REO loaded-plastic coacervates ($\sim 54\%w$) were successively elaborated indicating that the
654 BCac was successfully used to envelop the EO-charged micellar system. In addition, the
655 hydrophobic effect incited during the grafting reaction contributes highly in the formation of
656 stable coacervates, and that by the migration of water molecules around the oily hydrophobic
657 surface into the solution through the polymer chains (self-associated). The *Flory–Huggins*
658 thermodynamic theory was used to predict the demixation according to the DS value and
659 revealed the strong effect of DS on the molar Gibbs free energy of mixing values. However,
660 the polymer modification at the constant concentration affects strongly the interaction force
661 distribution of the cellulosic derivatives. Furthermore, beyond the critical chi-Flory value (χ_c),
662 corresponding to the critical DS-value (DS_c), the mixture Gibbs energy (ΔG_{mix}) values become
663 positive making demixing more favorable, this explains the formation of coacervates through
664 the “Pickering” membrane at the biphasic interfacial.

665 **Acknowledgements**

666 We thank greatly the anonymous reviewers for their careful review and valuable suggestions
667 on the manuscript. The authors are thankful to the Head of Oujda's chemistry department and

668 the Head of Physical Measurements, *Prof. Abdelmonaem TALHAOUI*, for providing all the
669 facilities and subsidies necessary to carry out the research work of this article, and to *Prof.*
670 *Boujamaa EL KOUY*, professor of English Language and Linguistics - FPN faculty for English
671 improvement. Our warm thanks are also addressed to *Prof. Mohamed LOUTOU*, Laboratory of
672 Molecular Chemistry, Materials and Environment (LMCME) FPN/UMP, for his sincere and
673 persistent contributions and devoted cooperation.

674 **References:**

- 675 Abderahmane E, El Barkany S, Hassan A, Abdel-Karim M (2011) Synthesis and characterization of the new
676 cellulose derivative films based on the hydroxyethyl cellulose prepared from “*Stipa tenacissima*” cellulose
677 of Eastern Morocco. I. Solubility Study. *J Appl Polym Sci* 122:2952–2965
- 678 Abdulkhani A, Marvast EH, Ashori A, Hamzeh Y, Karimi AN (2013) Preparation of cellulose/polyvinyl alcohol
679 biocomposite films using 1-n-butyl-3-methylimidazolium chloride. *Int J Biol Macromol* 62:379–386
- 680 Adonijah Graham S, Dudem B, Patnam H, Mule AR, Yu JS (2020) Integrated design of highly porous
681 celluloseloaded polymer-based triboelectric films toward flexible, humidity-resistant, and sustainable
682 mechanical energy harvesters. *ACS Energy Lett* 5:2140–2148
- 683 Amalraj A, Gopi S, Thomas S, Haponiuk JT (2018). Cellulose nanomaterials in biomedical, food, and nutraceutical
684 applications: a review. In: *Macromolecular Symposia*. Wiley Online Library
- 685 Amorim JD, Nascimento HA, Silva Junior CJG, Medeiros AD, Silva IDL, Costa AFS, Vinhas GM, Sarubbo LA
686 (2022) Obtainment of bacterial cellulose with added propolis extract for cosmetic applications. *Polym Eng*
687 *Sci* 62:565–575
- 688 Arshad M, Maaroufi A, Pinto G, El-Barkany S, Elidrissi A (2016) Morphology, thermal stability and thermal
689 degradation kinetics of cellulose-modified urea–formaldehyde resin. *Bull Mater Sci* 39:1609–1618
- 690 Aw YZ, Lim HP, Low LE, Singh CKS, Chan ES, Tey BT (2022) Cellulose nanocrystal (CNC)-stabilized Pickering
691 emulsion for improved curcumin storage stability. *LWT* 159:113249
- 692 Babkin V, Dmitriev VY, Titova E, Zaikov G (2012). Geometrical and electronic structure of molecule α -glucose
693 by method AB INITIO. In : *Quantum-chemical calculations of molecular systems as the basis of*
694 *nanotechnologies in applied quantum chemistry*, pp 7–11
- 695 Barbu E, de Carvalho RA, Amaral AC, Carvalho AJF, Trovatti E (2021) Conjugation of folic acid with TEMPO-
696 oxidized cellulose hydrogel for doxorubicin administration. *Carbohydr Polym Technol Appl* 2:100019
- 697 Barton AF (2017) *CRC handbook of solubility parameters and other cohesion parameters*. Routledge
- 698 Berruyer P, Gericke M, Moutzouri P, Jakobi D, Bardet M, Karlson L, Schantz S, Heinze T, Emsley L (2021)
699 Advanced characterization of regioselectively substituted methylcellulose model compounds by DNP
700 enhanced solidstate NMR spectroscopy. *Carbohydr Polym* 262:117944
- 701 Bertsch P, Schneider L, Bovone G, Tibbitt MW, Fischer P, Gstöhl S (2019) Injectable biocompatible hydrogels
702 from cellulose nanocrystals for locally targeted sustained drug release. *ACS Appl Mater Interfaces*
703 11:38578–38585
- 704 Brar AS, Kaur J (2005) 2D NMR studies of acrylonitrile–methyl acrylate copolymers. *Eur Polym J* 41:2278–2289
- 705 Breitzkreutz J (1998) Prediction of intestinal drug absorption properties by three-dimensional solubility parameters.
706 *Pharm Res* 15:1370–1375
- 707 Cadinoiu AN, Rata DM, Atanase LI, Daraba OM, Gherghel D, Vochita G, Popa M (2019) Aptamer-functionalized
708 liposomes as a potential treatment for basal cell carcinoma. *Polymers* 11:1515
- 709 Cadinoiu AN, Rata DM, Atanase LI, Mihai CT, Bacaita SE, Popa M (2021) Formulations based on drug loaded
710 aptamer-conjugated liposomes as a viable strategy for the topical treatment of basal cell carcinoma—in
711 vitro tests. *Pharmaceutics* 13:866
- 712 Calahorra M, Cortazar M, Eguiazábal J, Guzmán G (1989) Thermogravimetric analysis of cellulose: effect of the
713 molecular weight on thermal decomposition. *J Appl Polym Sci* 37:3305–3314
- 714 Carrillo-Varela I, Pereira M, Mendonça RT (2018) Determination of polymorphic changes in cellulose from
715 *Eucalyptus* spp. fibres after alkalization. *Cellulose* 25:6831–6845
- 716 Carvalho T, Guedes G, Sousa FL, Freire CS, Santos HA (2019) Latest advances on bacterial cellulose-based
717 materials for wound healing, delivery systems, and tissue engineering. *Biotechnol J* 14:1900059
- 718 Castellanos NL, Smaghe G, Sharma R, Oliveira EE, Christiaens O (2019) Liposome encapsulation and EDTA
719 formulation of dsRNA targeting essential genes increase oral RNAi-caused mortality in the Neotropical
720 stink bug *Euschistus heros*. *Pest Manag Sci* 75:537–548

721 Chaouf S, El Barkany S, Jilal I, El Ouardi Y, Abou-salama M, Loutou M, El-Houssaine A, El-Ouarghi H, El Idrissi
722 A, Amhamdi H (2019) Anionic reverse microemulsion grafting of acrylamide (AM) on
723 HydroxyEthylCellulose (HEC): synthesis, characterization and application as new ecofriendly low-cost
724 flocculant. *J Water Process Eng* 31:100807

725 Chaouf S, El Barkany S, Amhamdi H, Jilal I, El Ouardi Y, Abou-salama M, Loutou M, El-Houssaine A, El Ouarghi
726 H, El Idrissi A (2020) Low degree of substitution of cellulose acrylate based green polyelectrolyte:
727 synthesis, characterization and application to the removal of Cu(II) ions and colloidal Fe (OH) 3 turbidity.
728 *Mater Today Proc* 31:S175–S182

729 Chen H, Muros-Cobos JL, Amirfazli A (2018a) Contact angle measurement with a smartphone. *Rev Sci Instrum*
730 89:035117

731 Chen W, He H, Zhu H, Cheng M, Li Y, Wang S (2018b) Thermo-responsive cellulose-based material with
732 switchable wettability for controllable oil/water separation. *Polymers* 10:592

733 Chung CK, Beekmann U, Kralisch D, Bierau K, Chan A, Ossendorp F, Cruz LJ (2022) Bacterial cellulose as drug
734 delivery system for optimizing release of immune checkpoint blocking antibodies. *Pharmaceutics* 14:1351

735 Ciolacu DE, Nicu R, Ciolacu F (2020) Cellulose-based hydrogels as sustained drug-delivery systems. *Materials*
736 13:5270 Clasen C, Kulicke W-M (2001) Determination of viscoelastic and rheo-optical material functions
737 of water-soluble cellulose derivatives. *Prog Polym Sci* 26:1839–1919

738 Cullum BM, Vo-Dinh T (2003) Sample collection and preparation of liquid and solids. *Handb Spectrosc* 2:1 Dai
739 L, Cheng T, Wang Y, Lu H, Nie S, He H, Duan C, Ni Y (2019) Injectable all-polysaccharide self-
740 assembling hydrogel: a promising scaffold for localized therapeutic proteins. *Cellulose* 26:6891–6901

741 Damiri F, Kommineni N, Ebhodaghe SO, Bulusu R, Jyothi VGS, Sayed AA, Awaji AA, Germoush MO, Al-Malky
742 HS, Nasrullah MZ (2022) Microneedle-based natural polysaccharide for drug delivery systems (DDS):
743 progress and challenges. *Pharmaceutics* 15:190

744 de Amorim JDP, de Souza KC, Duarte CR, da Silva Duarte I, de Assis Sales Ribeiro F, Silva GS, de Farias PMA,
745 Stingl A, Costa AFS, Vinhas GM (2020) Plant and bacterial nanocellulose: production, properties and
746 applications in medicine, food, cosmetics, electronics and engineering: a review. *Environ Chem Lett*
747 18:851–869

748 De Oliveira JR, Camargo SEA, De Oliveira LD (2019) *Rosmarinus officinalis* L. (rosemary) as therapeutic and
749 prophylactic agent. *J Biomed Sci* 26:1–22

750 El Barkany S, El Idrissi A, Ouslimane S, Amhamdi H (2009) Optimization of the experimental conditions for the
751 extraction of cellulose starting from the “stipa tenacissima” of Eastern Morocco. *Phys Chem News* 46:135–
752 141

753 El Fawal GF, Omer AM, Tamer TM (2019) Evaluation of antimicrobial and antioxidant activities for cellulose
754 acetate films incorporated with Rosemary and Aloe Vera essential oils. *J Food Sci Technol* 56:1510–1518

755 El Idrissi A, El Barkany S, Amhamdi H, Maaroufi AK (2013) Synthesis and characterization of the new cellulose
756 derivative films based on the hydroxyethyl cellulose prepared from esparto “Stipa tenacissima” cellulose
757 of Eastern Morocco. II. Esterification with acyl chlorides in a homogeneous medium. *J Appl Polym Sci*
758 127:3633–3644

759 Fakoya S (2013) Antimicrobial activity of Cu, Ni carboxylates of castor (*Ricinus communis*) seed oil and their
760 calcinated derivatives. *J Appl Sci Environ Manag* 17:483–490

761 Feng J, Shi Y, Yu Q, Sun C, Yang G (2016) Effect of emulsifying process on stability of pesticide nanoemulsions.
762 *Colloids Surf Physicochem Eng Aspects* 497:286–292

763 Fukuta T, Kogure K (2022) Biomimetic nanoparticle drug delivery systems to overcome biological barriers for
764 therapeutic applications. *Chem Pharm Bull* 70:334–340

765 Garside P, Wyeth P (2003) Identification of cellulosic fibres by FTIR spectroscopy-thread and single fibre analysis
766 by attenuated total reflectance. *Stud Conserv* 48:269–275

767 Ghorbani S, Eyni H, Bazaz SR, Nazari H, Asl LS, Zaferani H, Kiani V, Mehrizi AA, Soleimani M (2018)
768 Hydrogels based on cellulose and its derivatives: applications, synthesis, and characteristics. *Polym Sci Ser*
769 A 60:707–722

770 Ghorbani Chaboki M, Mohammadi-Rovshandeh J, Hemmati F (2019) Poly (lactic acid)/thermoplasticized rice
771 straw biocomposites: effects of benzylated lignocellulosic filler and nanoclay. *Iran Polym J* 28:777–788

772 Gong F, Wang R, Chen X, Chen P, An Z, Zhang S (2017) Facile synthesis and the properties of novel cardo poly
773 (arylene ether sulfone) s with pendent cycloaminium side chains as anion exchange membranes. *Polym*
774 *Chem* 8:4207–4219

775 González-Vallinas M, Reglero G, Ramírez de Molina A (2015) Rosemary (*Rosmarinus officinalis* L.) extract as a
776 potential complementary agent in anticancer therapy. *Nutr Cancer* 67:1223–1231

777 Gu Z, Dong Y, Xu S, Wang L, Liu Z (2021) Molecularly imprinted polymer-based smart prodrug delivery system
778 for specific targeting, prolonged retention, and tumor microenvironment-triggered release. *Angew Chem*
779 133:2695–2699

780 Guo Y, Rockstraw DA (2007) Activated carbons prepared from rice hull by one-step phosphoric acid activation.
781 Microporous Mesoporous Mater 100:12–19

782 Guo Y, Wang X, Shu X, Shen Z, Sun R-C (2012) Selfassembly and paclitaxel loading capacity of cellulosegraft-
783 poly (lactide) nanomicelles. J Agric Food Chem 60:3900–3908

784 Guo Y, Liu Q, Chen H, Wang X, Shen Z, Shu X, Sun R (2013) Direct grafting modification of pulp in ionic liquids
785 and self-assembly behavior of the graft copolymers. Cellulose 20:873–884

786 Gupta B, Mishra V, Gharat S, Momin M, Omri A (2021) Cellulosic polymers for enhancing drug bioavailability
787 in ocular drug delivery systems. Pharmaceuticals 14:1201

788 Han W, Shin J, Shin JH (2022) Low-cost, open-source contact angle analyzer using a mobile phone, commercial
789 tripods and 3D printed parts. HardwareX 12:e00327

790 Hansen CM (1967) The three dimensional solubility parameter. Danish Tech Cpn 14 Hassabo AG, Mohamed AL,
791 Khattab TA (2022) Preparation of cellulose-based electrospun fluorescent nanofibres doped with perylene
792 encapsulated in silica nanoparticles for potential flexible electronics. Luminescence 37:21–27

793 Heinze T, Koschella A (2005) Solvents applied in the field of cellulose chemistry: a mini review. Polímeros 15:84–
794 90

795 Ho HN, Le HH, Le TG, Duong THA, Ngo VQT, Dang CT, Tran TH, Nguyen CN (2022) Formulation and
796 characterization of hydroxyethyl cellulose-based gel containing metronidazole-loaded solid lipid
797 nanoparticles for buccal mucosal drug delivery. Int J Biol Macromol 194:1010–1018

798 Hosseini M, Amiri M, Ghanbari M, Mahdi MA, Abdulsahib WK, Salavati-Niasari M (2022) Drug delivery based
799 on chitosan, β -cyclodextrin and sodium carboxymethyl cellulose as well as nanocarriers for advanced
800 leukemia treatment. Biomed Pharmacother 153:113369

801 Huang Y, Meng F, Liu R, Yu Y, Yu W (2019) Morphology and supramolecular structure characterization of
802 cellulose isolated from heat-treated moso bamboo. Cellulose 26:7067–7078

803 Huang W, Tang X, Qiu Z, Zhu W, Wang Y, Zhu Y-L, Xiao Z, Wang H, Liang D, Li J (2020) Cellulose-based
804 superhydrophobic surface decorated with functional groups showing distinct wetting abilities to manipulate
805 water harvesting. ACS Appl Mater Interfaces 12:40968–40978

806 Huo Y, Liu Y, Xia M, Du H, Lin Z, Li B, Liu H (2022) Nanocellulose- based composite materials used in drug
807 delivery systems. Polymers 14:2648

808 Ibarra A, Cases J, Bily A, He K, Bai N, Roller M, Coussaert A, Ripoll C (2010) Importance of extract
809 standardization and in vitro/ex vivo assay selection for the evaluation of antioxidant activity of botanicals:
810 a case study on three Rosmarinus officinalis L. extracts. J Med Food 13:1167–1175

811 Isogai A, Kato T, Uryu T, Atalla R (1993) Solid-state CP/MAS ¹³C-NMR analysis of cellulose and tri-O-
812 substituted cellulose ethers. Carbohydr Polym 21:277–281

813 Ivanova N, Gugleva V, Dobreva M, Pehlivanov I, Stefanov S, Andonova V (2018) Silver nanoparticles as multi-
814 functional drug delivery systems. IntechOpen, London

815 Jabir L, El-Hammi H, Mohammed N, Jilal I, El Idrissi A, Amhamdi H, Abou-Salama M, El Ouardi Y, El Barkany
816 S, Laatikainen K (2022) Cellulose based pH-sensitive hydrogel for highly efficient dye removal in water
817 treatment: kinetic, thermodynamic, theoretical and computational studies. Cellulose 29:4539–4564

818 Jain DD, Tambe SM, Amin PD (2022) Formulation performance window for manufacturing cellulose-based
819 sustained-release mini-matrices of highly water-soluble drug via hot-melt extrusion technology. Cellulose
820 29:3323–3350

821 Janmohammadi M, Nazemi Z, Salehi AOM, Seyfoori A, John JV, Nourbakhsh MS, Akbari M (2023) Cellulose-
822 based composite scaffolds for bone tissue engineering and localized drug delivery. Bioact Mater 20:137–
823 163

824 Jilal I, El Barkany S, Bahari Z, Sundman O, El Idrissi A, Abou- Salama M, Romane A, Zannagui C, Amhamdi H
825 (2018a) New quaternized cellulose based on hydroxyethyl cellulose (HEC) grafted EDTA: synthesis,
826 characterization and application for Pb(II) and Cu(II) removal. Carbohydr Polym 180:156–167

827 Jilal I, El Barkany S, Bahari Z, Sundman O, El Idrissi A, Salhi A, Abou-Salama M, Loutou M, Amhamdi H
828 (2018b) Unconventional synthesis, characterization and theoretical study (HF and DFT computations) of
829 new cellulosic copper complex: benzyloxyethyl cellulose copper (CuBEC). Cellulose 25:4375–4388

830 Jilal I, El-Barkany S, Bahari Z, Sundman O, El-Idrissi A, Abou-Salama M, Loutou M, Ablouh E, Amhamdi H
831 (2019) New benzyloxyethyl cellulose (BEC) crosslinked EDTA: synthesis, characterization and application
832 for supramolecular self-assembling nanoencapsulation of Pb (II). Mater Today Proc 13:909–919

833 Jilal I, El Barkany S, Bahari Z, El Ouardi Y, Loutou M, Amhamdi H, Abou-Salama M, Salhi A, El Idrissi A,
834 Laatikainen K (2021) New ethylenediamine crosslinked 2D-cellulose adsorbent for nanoencapsulation
835 removal of Pb(II) and Cu(II) heavy metal ions: synthesis, characterization application, and RSM-modeling.
836 Cellulose Science and Derivatives, IntechOpen

837 Johar N, Ahmad I, Dufresne A (2012) Extraction, preparation and characterization of cellulose fibres and
838 nanocrystals from rice husk. Ind Crops Prod 37:93–99

839 Johnson A, Kong F, Miao S, Lin H-TV, Thomas S, Huang Y-C, Kong Z-L (2020) Therapeutic effects of antibiotics
840 loaded cellulose nanofiber and κ -carrageenan oligosaccharide composite hydrogels for periodontitis
841 treatment. *Sci Rep* 10:1–23

842 Karimian A, Parsian H, Majidinia M, Rahimi M, Mir SM, Kafil HS, Shafiei-Irannejad V, Kheyrollah M, Ostadi
843 H, Yousefi B (2019) Nanocrystalline cellulose: preparation, physicochemical properties, and applications
844 in drug delivery systems. *Int J Biol Macromol* 133:850–859

845 Karimian A, Yousefi B, Sadeghi F, Feizi F, Najafzadehvarzi H, Parsian H (2022) Synthesis of biocompatible
846 nanocrystalline cellulose against folate receptors as a novel carrier for targeted delivery of doxorubicin.
847 *Chem Biol Interact* 351:109731

848 Kesharwani P, Kumari K, Gururani R, Jain S, Sharma S (2022) Approaches to address PK-PD Challenges of
849 conventional liposome formulation with special reference to cancer, Alzheimer's, diabetes, and glaucoma:
850 an update on modified liposomal drug delivery system. *Curr Drug Metab*

851 Khalil HA, Yahya EB, Jummaat F, Adnan A, Olaiya N, Rizal S, Abdullah C, Pasquini D, Thomas S (2022)
852 Biopolymers based aerogels: a review on revolutionary solutions for smart therapeutics delivery. *Prog*
853 *Mater Sci* 131:101014

854 Kim MS, Park SJ, Gu BK, Kim C-H (2012) Ionically crosslinked alginate–carboxymethyl cellulose beads for the
855 delivery of protein therapeutics. *Appl Surf Sci* 262:28–33

856 Kim Y, Jeong D, Park KH, Yu J-H, Jung S (2018) Efficient adsorption on benzoyl and stearoyl cellulose to remove
857 phenanthrene and pyrene from aqueous solution. *Polymers* 10:1042

858 King AW, Mäkelä V, Kedzior SA, Laaksonen T, Partl GJ, Heikkinen S, Koskela H, Heikkinen HA, Holding AJ,
859 Cranston ED (2018) Liquid-state NMR analysis of nanocelluloses. *Biomacromol* 19:2708–2720

860 Klębowski B, Depciuch J, Parlińska-Wojtan M, Baran J (2018) Applications of noble metal-based nanoparticles
861 in medicine. *Int J Mol Sci* 19:4031

862 Knop S, Jansen TLC, Lindner J, Vöhringer P (2011) On the nature of OH-stretching vibrations in hydrogen-bonded
863 chains: pump frequency dependent vibrational lifetime. *Phys Chem Chem Phys* 13:4641–4650

864 Kono H, Hashimoto H, Shimizu Y (2015) NMR characterization of cellulose acetate: chemical shift assignments,
865 substituent effects, and chemical shift additivity. *Carbohydr Polym* 118:91–100

866 Kortüm G (1961) Dissociation constants of organic acids in aqueous solution. Butterworth Kortüm G, Vogel W,
867 Andrussow AK (1960) Dissociation constants of organic acids in aqueous solution. *Pure Appl Chem*
868 1:187–536

869 Krevelen DW (1972) Properties of polymers: correlations with chemical structure. Elsevier

870 Krivoshein AV, Ordonez C, Khrustalev VN, Timofeeva TV (2016) Distinct molecular structures and hydrogen
871 bond patterns of α , α -diethyl-substituted cyclic imide, lactam, and acetamide derivatives in the crystalline
872 phase. *J Mol Struct* 1121:196–202

873 Kulkarni N, Jain P, Shindikar A, Suryawanshi P, Thorat N (2022) Advances in the colon-targeted chitosan based
874 drug delivery systems for the treatment of inflammatory bowel disease. *Carbohydr Polym* 288:119351

875 Kumari P, Raza W, Meena A (2021) Lemongrass derived cellulose nanofibers for controlled release of curcumin
876 and its mechanism of action. *Ind Crops Prod* 173:114099

877 Li J, Zhang L-P, Peng F, Bian J, Yuan T-Q, Xu F, Sun R-C (2009) Microwave-assisted solvent-free acetylation of
878 cellulose with acetic anhydride in the presence of iodine as a catalyst. *Molecules* 14:3551–3566

879 Lindvig T, Michelsen ML, Kontogeorgis GM (2001) Thermodynamics of paint-related systems with engineering
880 models. *AIChE J* 47:2573–2584

881 Liu Y, Ahmed S, Sameen DE, Wang Y, Lu R, Dai J, Li S, Qin W (2021) A review of cellulose and its derivatives
882 in biopolymer-based for food packaging application. *Trends Food Sci Technol* 112:532–546

883 Liu Z, Zhang S, Gao C, Meng X, Wang S, Kong F (2022) Temperature/pH-responsive carboxymethyl cellulose/
884 poly (N-isopropyl acrylamide) interpenetrating polymer network aerogels for drug delivery systems.
885 *Polymers* 14:1578

886 Low LE, Tan LT-H, Goh B-H, Tey BT, Ong BH, Tang SY (2019) Magnetic cellulose nanocrystal stabilized
887 Pickering emulsions for enhanced bioactive release and human colon cancer therapy. *Int J Biol Macromol*
888 127:76–84

889 Lu Q-l, Li X-y, Tang L-r, Lu B-l, Huang B (2015) One-pot tandem reactions for the preparation of esterified
890 cellulose nanocrystals with 4-dimethylaminopyridine as a catalyst. *RSC Adv* 5:56198–56204

891 Lukova P, Katsarov P, Pilicheva B (2023) Application of starch, cellulose, and their derivatives in the development
892 of microparticle drug-delivery systems. *Polymers* 15:3615

893 Lv Z, He S, Wang Y, Zhu X (2021) Noble metal nanomaterials for NIR-triggered photothermal therapy in cancer.
894 *Adv Healthc Mater* 10:2001806

895 Ma T, Cui R, Lu S, Hu X, Xu B, Song Y, Hu X (2022) High internal phase Pickering emulsions stabilized by
896 cellulose nanocrystals for 3D printing. *Food Hydrocoll* 125:107418

897 Maafi EM, Malek F, Tighzert L, Dony P (2010) Synthesis of polyurethane and characterization of its composites
898 based on alfa cellulose fibers. *J Polym Environ* 18:638–646

899 Mbituyimana B, Liu L, Ye W, Boni BOO, Zhang K, Chen J, Thomas S, Vasilievich RV, Shi Z, Yang G (2021)
900 Bacterial cellulose-based composites for biomedical and cosmetic applications: research progress and
901 existing products. *Carbohydr Polym* 273:118565

902 Mehta S, MacGillivray M (2022) Aromatherapy in textiles: a systematic review of studies examining textiles as a
903 potential carrier for the therapeutic effects of essential oils. *Textiles* 2:29–49

904 Miyamoto T, Sato Y, Shibata T, Tanahashi M, Inagaki H (1985) ¹³C-NMR spectral studies on the distribution of
905 substituents in water-soluble cellulose acetate. *J Polym Sci Polym Chem Ed* 23:1373–1381

906 Miyamoto T, Long M, Donkai N (1995) Preparation of new types of temperature-responsive cellulose derivatives.
907 In: *Macromolecular symposia*, Wiley

908 Mohan T, Ajdnik U, Nagaraj C, Lackner F, Dobaj Štiglic A, Palani T, Amornkitbamrung L, Gradišnik L, Maver
909 U, Kargl R (2022) One-step fabrication of hollow spherical cellulose beads: application in pH-responsive
910 therapeutic delivery. *ACS Appl Mater Interfaces* 14:3726–3739

911 Molenveld K, Slaghek TM (2022) Recent developments in biodegradable cellulose-based plastics. In:
912 *Biodegradable polymers in the circular plastics economy*, pp 273–298

913 Nabipour H, Mansoorianfar M, Hu Y (2022) Carboxymethyl cellulose-coated HKUST-1 for baclofen drug
914 delivery in vitro. *Chem Papers* 1–10

915 Nascimento HA, Amorim JD, M. Filho LE, Costa AFS, Sarubbo LA, Napoleão DC, Maria Vinhas G (2022)
916 Production of bacterial cellulose with antioxidant additive from grape residue with promising cosmetic
917 applications. *Polym Eng Sci*

918 Niederquell A, Stoyanov E, Kuentz M (2022) Hydroxypropyl cellulose for drug precipitation inhibition: from the
919 potential of molecular interactions to performance considering microrheology. *Mol Pharm* 19:690–703

920 Nsor-Atindana J, Chen M, Goff HD, Zhong F, Sharif HR, Li Y (2017) Functionality and nutritional aspects of
921 microcrystalline cellulose in food. *Carbohydr Polym* 172:159–174

922 O'Brien CT, Virtanen T, Donets S, Jennings J, Guskova O, Morrell AH, Rymaruk M, Ruusuvirta L, Salmela J,
923 Setälä H (2021) Control of the aqueous solubility of cellulose by hydroxyl group substitution and its effect
924 on processing. *Polymer* 223:123681

925 Panda H (2005). *Aromatic plants cultivation, processing and uses: how to start a successful aromatic plants
926 business, How to start aromatic plants cultivation industry in India, How to start aromatic plants farm?,
927 How to start aromatic plants production business, Indian aromatic plant, List of aromatic plants and their
928 uses*, Asia Pacific Business Press Inc.

929 Pappas C, Tarantilis P, Daliani I, Mavromoustakos T, Polissiou M (2002) Comparison of classical and
930 ultrasound-assisted isolation procedures of cellulose from kenaf (*Hibiscus cannabinus* L.) and eucalyptus
931 (*Eucalyptus rostratus* Sm.). *Ultrason Sonochem* 9:19–23

932 Popa L, Ghica MV, Tudoroiu E-E, Ionescu D-G, Dinu-Pirvu C-E (2022) Bacterial cellulose—a remarkable
933 polymer as a source for biomaterials tailoring. *Materials* 15:1054

934 Prigogine I, Mathot V, Bellemans A (1957) Molecular theory of solutions Qi H, Liebert T, Heinze T (2012)
935 Homogenous synthesis of 3-allyloxy-2-hydroxypropyl-cellulose in NaOH/urea aqueous system. *Cellulose*
936 19:925–932

937 Qiao L, Yang H, Gao S, Li L, Fu X, Wei Q (2022) Research progress on self-assembled nanodrug delivery systems.
938 *J Mater Chem B*

939 Raghav N, Sharma MR, Kennedy JF (2021) Nanocellulose: a mini-review on types and use in drug delivery
940 systems. *Carbohydr Polym Technol Appl* 2:100031

941 Rață DM, Cadinoiu AN, Atanase LI, Bacaita SE, Mihalache C, Daraba O-M, Gherghel D, Popa M (2019) “In
942 vitro” behaviour of aptamer-functionalized polymeric nanocapsules loaded with 5-fluorouracil for targeted
943 therapy. *Mater Sci Eng C* 103:109828

944 Rata DM, Cadinoiu AN, Atanase LI, Popa M, Mihai C-T, Solcan C, Ochiuz L, Vochita G (2021) Topical
945 formulations containing aptamer-functionalized nanocapsules loaded with 5-fluorouracil—an innovative
946 concept for the skin cancer therapy. *Mater Sci Eng C* 119:111591

947 Ravindra R, Krovvidi KR, Khan A (1998) Solubility parameter of chitin and chitosan. *Carbohydr Polym* 36:121–
948 127

949 Raza A, Kamato D, Sime F, Roberts J, Popat A, Falconer J, Kumeria T (2022) Influence of PEGylated porous
950 silicon nanoparticles on permeation and efflux of an orally administered antibiotic. *Mater Today Adv*
951 13:100210

952 Razavi MS, Golmohammadi A, Nematollahzadeh A, Rovera C, Farris S (2022) Cinnamon essential oil
953 encapsulated into a fish gelatin-bacterial cellulose nanocrystals complex and active films thereof. *Food*
954 *Biophys* 17:38–46

955 Rezaei A, Rafieian F, Akbari-Alavijeh S, Kharazmi MS, Jafari SM (2022) Release of bioactive compounds from
956 delivery systems by stimuli-responsive approaches; triggering factors, mechanisms, and applications. *Adv*
957 *Colloid Interface Sci* 307:102728

958 Ribea J, Skov N, Kavlia O, Håtia A, Bruusb H, Stokkea B (2016) Simple and low-cost contact angle measurements
959 using a smartphone with a PDMS-Lens. *Chips and Tips: R. Soc. Chem.* See [https:// blogs. rsc. org/ chips](https://blogs.rsc.org/chips)
960 [andti ps/ 2016/ 07/ 19/ simple- and- low- cost- conta ct- angle- measu remen ts- using-a- smart phone- with-](https://blogs.rsc.org/chips/2016/07/19/simple-and-low-cost-contact-angle-measurements-using-a-smartphone-with-a-pdms-lens/)
961 [a- pdms- lens/](https://blogs.rsc.org/chips/2016/07/19/simple-and-low-cost-contact-angle-measurements-using-a-smartphone-with-a-pdms-lens/) .[Google Scholar]

962 Rodríguez-Rojo S, Varona S, Núñez M, Cocero M (2012) Characterization of rosemary essential oil for
963 biodegradable emulsions. *Ind Crops Prod* 37:137–140

964 Saito Y, Shiga A, Yoshida Y, Furuhashi T, Fujita Y, Niki E (2004) Effects of a novel gaseous antioxidative system
965 containing a rosemary extract on the oxidation induced by nitrogen dioxide and ultraviolet radiation. *Biosci*
966 *Biotechnol Biochem* 68:781–786

967 Saliu OD, Olatunji GA, Yakubu A, Arowona MT, Mohammed AA (2017) Catalytic crosslinking of a regenerated
968 hydrophobic benzylated cellulose and nano TiO₂ composite for enhanced oil absorbency. *E-Polymers*
969 17:295–302

970 Schnabelrauch M, Vogt S, Klemm D, Nehls I, Philipp B (1992) Readily hydrolyzable cellulose esters as
971 intermediates for the regioselective derivatization of cellulose, 1. Synthesis and characterization of soluble,
972 low-substituted cellulose formates. *Die Angew Makromol Chem Appl Macromol Chem Phys* 198:155–164

973 Sheng K, Zhang G, Kong X, Wang J, Mu W, Wang Y (2021a) Encapsulation and characterisation of grape seed
974 proanthocyanidin extract using sodium alginate and different cellulose derivatives. *Int J Food Sci Technol*
975 56:6420–6430

976 Sheng Y, Gao J, Yin Z-Z, Kang J, Kong Y (2021b) Dual-drug delivery system based on the hydrogels of alginate
977 and sodium carboxymethyl cellulose for colorectal cancer treatment. *Carbohydr Polym* 269:118325

978 Shi Y-X, Li S-H, Zhao Z-P (2022) Molecular simulations of the effects of substitutions on the dissolution
979 properties of amorphous cellulose acetate. *Carbohydr Polym* 291:119610

980 Smaoui S, Hlima HB, Tavares L, Ennouri K, Braiek OB, Mellouli L, Abdelkafi S, Khaneghah AM (2022)
981 Application of essential oils in meat packaging: a systemic review of recent literature. *Food Control*
982 132:108566

983 Song J, Liu M, Yang Z, Xu S, Cheng B, Fei P (2017) Synthesis and characterization of cellulose acetate naphthoate
984 with good ultraviolet and chemical resistance. *E-Polymers* 17:333–340

985 Su C, Liu Y, Li R, Wu W, Fawcett JP, Gu J (2019) Absorption, distribution, metabolism and excretion of the
986 biomaterials used in nanocarrier drug delivery systems. *Adv Drug Del Rev* 143:97–114

987 Subramanian DA, Langer R, Traverso G (2022) Mucus interaction to improve gastrointestinal retention and
988 pharmacokinetics of orally administered nano-drug delivery systems. *J Nanobiotechnol* 20:1–23

989 Sukumaran NP, Gopi S (2021) Overview of biopolymers: resources, demands, sustainability, and life cycle
990 assessment modeling and simulation. In: *Biopolymers and their industrial applications*, Elsevier, pp 1–19

991 Tatzber M, Stemmer M, Spiegel H, Katzlberger C, Haberhauer G, Mentler A, Gerzabek MH (2007) FTIR-
992 spectroscopic characterization of humic acids and humin fractions obtained by advanced NaOH, Na₄P₂O₇,
993 and Na₂CO₃ extraction procedures. *J Plant Nutr Soil Sci* 170:522–529

994 Van Krevelen D (1972) Correlations with chemical structure. *Properties of Polymers* 135–143

995 Van Krevelen DW, Te Nijenhuis K (2009) Properties of polymers: their correlation with chemical structure; their
996 numerical estimation and prediction from additive group contributions. Elsevier

997 Vickers NJ (2017) Animal communication: When I'm calling you, will you answer too? *Curr Biol* 27:R713–R715

998 Wang C, Chen SL (2005) Aromachology and its application in the textile field. *Fibres Text East Eur* 13:41–44

999 Weiss AM, Macke N, Zhang Y, Calvino C, Esser-Kahn AP, Rowan SJ (2021) In vitro and in vivo analyses of the
1000 effects of source, length, and charge on the cytotoxicity and immunocompatibility of cellulose nanocrystals.
1001 *ACS Biomater Sci Eng* 7:1450–1461

1002 Wen Y, Oh JK (2015) Intracellular delivery cellulose-based bionanogels with dual temperature/pH-response for
1003 cancer therapy. *Colloids Surf B Biointerfaces* 133:246–253

1004 Wijaya CJ, Ismadji S, Gunawan S (2021) A review of lignocellulosic- derived nanoparticles for drug delivery
1005 applications: lignin nanoparticles, xylan nanoparticles, and cellulose nanocrystals. *Molecules* 26:676

1006 Yamauchi G, Riko Y, Yasuno Y, Shimizu T, Funakoshi N (2005) Water-repellent coating for mobile phone
1007 microphones. *Surf Coat Int Part B Coat Trans* 88:281–283

1008 Yan L, Tao H, Bangal PR (2009) Synthesis and flocculation behavior of cationic cellulose prepared in a
1009 NaOH/urea aqueous solution. *Clean-Soil Air Water* 37:39–44

1010 Yuan S, Tyufekchiev MV, Timko MT, Schmidt-Rohr K (2022) Direct quantification of the degree of
1011 polymerization of hydrolyzed cellulose by solid-state NMR spectroscopy. *Cellulose* 29:2131–2144

1012 Zhang L, Chen Q, Ma Y, Sun J (2019) Microfluidic methods for fabrication and engineering of nanoparticle drug
1013 delivery systems. *ACS Appl Bio Mater* 3:107–120

1014 Zhang W, Liu Y, Xuan Y, Zhang S (2022) Synthesis and applications of carboxymethyl cellulose hydrogels. *Gels*
1015 8:529

- 1016 Zoia L, Morelli A, Talamini L, Violatto MB, Lovati AB, Lopa S, Recordati C, Toffanin C, Salanti A, Russo L
1017 (2020) Cellulose nanocrystals: a multimodal tool to enhance the targeted drug delivery against bone
1018 disorders. *Nanomedicine* 15:2271–2285
1019 Zuppolini S, Salama A, Cruz-Maya I, Guarino V, Borriello A (2022) Cellulose amphiphilic materials: chemistry.
1020 *Process Appl Pharm* 14:386